Pergamon

DEEP-SEA RESEARCH
PART I

Deep-Sea Research I 45 (1998) 673–717

Carbon-13 constraints on the seasonal inorganic carbon budget at the BATS site in the northwestern Sargasso Sea

Nicolas Gruber[a,*], Charles D. Keeling[b], Thomas F. Stocker[c]

[a] *Climate and Environmental Physics, Physics Institute, University of Bern, Bern, Switzerland*
[b] *Scripps Institution of Oceanography, University of California, San Diego, CA, USA*
[c] *Climate and Environmental Physics, Physics Institute, University of Bern, Bern, Switzerland*

Received 30 December 1996; received in revised form 14 July 1997; accepted 23 September 1997

Abstract

The seasonal budget of dissolved inorganic carbon (C) in the mixed layer at the U.S. JGOFS Bermuda Atlantic Time-series Study (BATS) site is assessed on the basis of a 4-yr time series (1991–1994) of high-precision C, alkalinity and the $^{13}C/^{12}C$ ratio of C. Compared to previous studies, our budget is constrained by observed changes in $^{13}C/^{12}C$, which permit calculation of the net community production. We are thus able to quantitatively separate all processes that contribute to the observed seasonal cycle in the mixed layer. Uncertainties in the C budget are determined using a Monte Carlo method. We found that net community production is mainly responsible in generating the observed C drawdown of about 26 $\mu mol\,kg^{-1}$ between April and October by removing on the average $-40 \pm 4\,\mu mol\,kg^{-1}$ from the mixed layer. This net community production occurs in the absence of measurable nitrate and phosphate concentrations. We hypothesize that N_2 fixation in combination with vertical migration may be large enough to meet the biological nutrient demand in the mixed layer during this summer/fall period. Physical processes do not explain the observed summer/fall drawdown except when very improbably large horizontal advective velocities are assumed. Annual net community production of $2.3 \pm 0.9\,mol\,m^{-2}$ is not well constrained by $^{13}C/^{12}C$, but if tentatively extrapolated to the whole euphotic layer, it is well within the range of estimates based on a wide variety of methods. The region around BATS is computed to be a moderate sink for atmospheric CO_2 with an annual uptake of $1.8 \pm 0.5\,mol\,m^{-2}$, with about 25% of this influx associated with the uptake of anthropogenic CO_2.

* Corresponding author. Fax: 0041 31 631 4405; e-mail: gruber@climate.unibe.cl.

0967-0637/98/$19.00
PII: S0967-0637(97)00098-8

1. Introduction

Most models that have been used to estimate the uptake of anthropogenic CO_2 by the oceans assume that the natural carbon cycle processes were in steady state before the onset of the man-made perturbation and since have continued to operate unchanged (Siegenthaler and Sarmiento, 1993). This assumption permits one to model the CO_2 uptake using a perturbation approach and, in particular, to neglect the influence of marine biology on the cycling of carbon in the ocean (Maier-Reimer and Hasselmann, 1987; Sarmiento *et al*., 1992; Siegenthaler and Joos, 1992; Stocker *et al*., 1994; Toggweiler, 1994a). In order to give reliable results, the models have only attempted to simulate vertical water transport correctly, since this transport is regarded as the main rate-determining step in sequestering anthropogenic CO_2 (Siegenthaler and Sarmiento, 1993). While the assumption of steady state for the natural carbon cycle is probably reasonable on the global scale for the present and the last 200 years (Broecker, 1991), models have shown that feedback mechanisms related to global warming can lead to changes in ocean circulation (Manabe and Stouffer, 1993; Stocker and Schmittner, in press) and hence also in the natural carbon cycle (Sarmiento, 1991; Sarmiento and LeQuéré, 1996; Maier-Reimer *et al*., 1996). Thus, in order to understand the processes that govern the exchange of CO_2 between the ocean and the atmosphere and eventually also the atmospheric CO_2 concentration, the complete natural carbon cycle in the ocean needs to be investigated (Sarmiento, 1991; Toggweiler, 1994a).

One means to address this issue is the establishment of time-series study sites in key regions of the world oceans (SCOR, 1987). A main goal of such studies is directed towards the understanding of the seasonal and interannual variability of inorganic carbon in the upper ocean. Seasonal variability represents a balance between physical processes (air–sea gas exchange, vertical mixing, and horizontal advection) and biological processes (photosynthetic uptake of CO_2, and its cycling through the food web, as well as the formation and dissolution of carbonate shells). One of the selected sites is the U.S. Joint Global Ocean Flux Study (JGOFS) Bermuda Atlantic Time-series Study (BATS) site at 31°50′N, 64°10′W in the oligotrophic northwestern Sargasso Sea (see map in Michaels and Knap (1996)). This part of the Sargasso Sea is an area of weak Gulf Stream recirculation with a net flow of less than 0.05 m s^{-1} towards the southwest (Michaels and Knap, 1996; Siegel and Deuser, 1997). The region is characterized by strong meridional gradients in hydrography and biological properties (Siegel *et al*., 1990). To the north of Bermuda, deep winter mixed layers of around 400 m occur nearly every year forming subtropical mode water (18° Water) by deep convection (Worthington, 1959; Talley and Raymer, 1982). This vertical overturning entrains nutrient rich waters from below, giving rise to a short lived vernal phytoplankton bloom (Siegel *et al*., 1990). South of Bermuda waters are permanently stratified, such that the mixed layer rarely extends below 100–150 m (Michaels and Knap, 1996). This weak vertical mixing leads to an ecosystem with all the characteristics of oligotrophy throughout the year. Either of these seasonal patterns can occur at the BATS site, depending on the intensity of winter mixing (Menzel and Ryther, 1960; Menzel and Ryther, 1961; Lohrenz *et al*., 1992; Michaels *et al*., 1994a, b; Michaels and Knap, 1996).

A quite unexpected observation in the area near Bermuda is the summer/fall drawdown of dissolved inorganic carbon (C) that occurs every year in the surface mixed layer in the absence of measurable nitrate and phosphate concentrations (Keeling, 1993; Bates *et al.*, 1996a, b; Lueker *et al.*, 1997). Modeling studies and the observation of a concomitant enrichment of surface C in ^{13}C (Keeling, 1993; Lueker *et al.*, 1997) point to net community production (gross primary production minus community respiration (Williams, 1993)) as the most important process (Marchal *et al.*, 1996; Bates *et al.*, 1996b). It has been suggested, however, that horizontal advection may also play an important role (Toggweiler, 1994b; Michaels *et al.*, 1994a, b; Bates *et al.*, 1996b). The estimated net community production of Marchal *et al.* (1996) and Bates *et al.* (1996b) has been computed by difference from the observed drawdown of C, taking into account the contributions of air–sea gas exchange and vertical mixing. Lacking an independent check on the consistency of the calculations, the uncertainty in estimating net community production is therefore directly proportional to the combined uncertainties of the other processes considered.

The purpose of this paper is to present a diagnostic technique utilizing isotopic data to estimate the magnitude of net community production. This technique is based on the observed variability of the $^{13}C/^{12}C$ ratio of C and on independent estimates of the magnitude of physical processes such as air–sea gas exchange, vertical diffusion, entrainment and horizontal advection. Adopting this technique permits us to quantitatively deduce the contribution of these processes, allowing comparison of the computed temporal evolution of C with the observed variability to evaluate the consistency of the calculations. We apply this diagnostic technique to our inorganic carbon system observations obtained at the U.S. JGOFS BATS station between 1991 and 1994. These observations include the shore-based high-precision determination of the concentration of dissolved inorganic carbon (C), alkalinity (Alk) and of the $^{13}C/^{12}C$ ratio of C. Since these observations pertain to the mixed layer only, additional measurements performed by the Bermuda Biological Station for Research (Bates *et al.*, 1996b) will be used to obtain information about the C distribution in the upper 250 m of the ocean. Our study extends the previous works of Marchal *et al.* (1996) and Bates *et al.* (1996b) in three respects. First, isotopic data are now available to estimate net community production directly. A consistency check of this estimate can thus be performed. Second, the role of advection is explicitly taken into account, although its magnitude is still very uncertain. Finally, we investigate quantitatively the entire seasonal cycle and not just the summer/fall period. The employed model here is an extended and improved version of an earlier box model developed by Gruber and Keeling (1998), which has been already partially presented by Keeling (1993). This earlier model has been used diagnostically to analyze carbon system observations at the nearby ocean station 'S' (32°10′N, 64°30′W) from 1983 to 1989. Improvements to the previous model consist of a more realistic parameterization of entrainment, explicit inclusion of an advection term, and Monte Carlo simulations to assess better the potential uncertainties in the estimated carbon budget.

The paper is organized as follows: In the first section we describe briefly the seasonal carbon system observations obtained at BATS between 1990 and 1994, which will form the input to the diagnostic model. We then present the model equations and

show how the various input variables and parameters of the model have been determined. The method section ends with a presentation of the numerical implementation and of the Monte Carlo analysis, which is used to assess model uncertainties. The results are then presented and discussed in comparison with previous studies in the Sargasso Sea.

2. Mixed layer carbon system observations

Since June 1990, personnel from the Bermuda Biological Station for Research (BBSR) sampled the sea water at the BATS station for us in duplicate at approximately 2 and 10 m depth. The bottles were then shipped to the laboratory of the Carbon Dioxide Research Group (CDRG) of the Scripps Institution of Oceanography. The samples were analyzed for dissolved inorganic carbon (C), total titration alkalinity (Alk) and the $^{13}C/^{12}C$ ratio of C following the procedures described in detail by Lueker *et al.* (1997) and summarized in Appendix A. The fugacity of CO_2 in the water, fCO_2^{oc}, was calculated from C, Alk, temperature, salinity and nutrients using the routine of Fink (1996). Computed fCO_2^{oc} values were reduced by 13 μatm, based on a comparison of direct measurements of fCO_2^{oc} at sea (see Appendix A and Lueker *et al.* (1997)).

The set of the CDRG carbon observations for water samples collected at BATS for the years 1990–1994 (BATS 21–BATS 75) is shown in Fig. 1. Also shown in Fig. 1 are the data obtained by Bates *et al.* (1996b) to permit a direct comparison. Both C and Alk data have been normalized to the annual mean mixed layer salinity of 36.6 to remove the effect of evaporation and precipitation (we express salinity on the practical salinity scale, which has no units (UNESCO, 1981)).

Normalized C in the mixed layer shows a distinct seasonal cycle with an amplitude of about 30–40 μmol kg^{-1} (Fig. 1a). This cycle is very similar in amplitude and phase to the seasonal pattern observed at station 'S' since 1983 (Keeling, 1993; Lueker *et al.*, 1997). Bates *et al.* (1996b) identified four different characteristic periods, which are observed nearly every year: (i) a winter–spring (February–April) maximum, (ii) a spring–summer (May–August) drawdown, (iii) a late summer–fall minimum (August–October) and (iv) an increase of C in fall to early winter (October–January). Interannual variability is relatively small compared to the large seasonal cycle and is mainly

Fig. 1. Seasonal variations of the measured parameters of the inorganic carbon system at BATS from 1990 to 1994. (a) Dissolved inorganic carbon (C) in μmol kg^{-1} normalized to a constant salinity of 36.6 (annual mean salinity at BATS) measured at approximately 2 and 10 m depth by the Carbon Dioxide Research Group (CDRG) (open and filled circles). Also shown are the mean C concentration in the upper 20 m as measured by the Bermuda Biological Station for Research (BBSR) (Michaels *et al.*, 1994a, b; Bates *et al.*, 1996a; Bates *et al.*, 1996b) (diamonds). (b) Total alkalinity (Alk) in μmol kg^{-1} normalized to a constant salinity of 36.6 measured at approximately 2 and 10 m depth by CDRG (open and filled circles). The mean BBSR Alk in the upper 20 m for the same period are shown by diamonds (Bates *et al.*, 1996a, b) (c) $\delta^{13}C$ in ‰, measured by CDRG at approximately 10 m depth. (d) Calculated CO_2 fugacity in the mixed layer in μatm based on the CDRG carbon data at approximately 2 and 10 m depth (open and filled circles). The computed fCO_2^{oc} were reduced by 13 μatm to agree closely with direct observations. The calculated fCO_2^{oc} of BBSR in μatm are shown by diamonds.

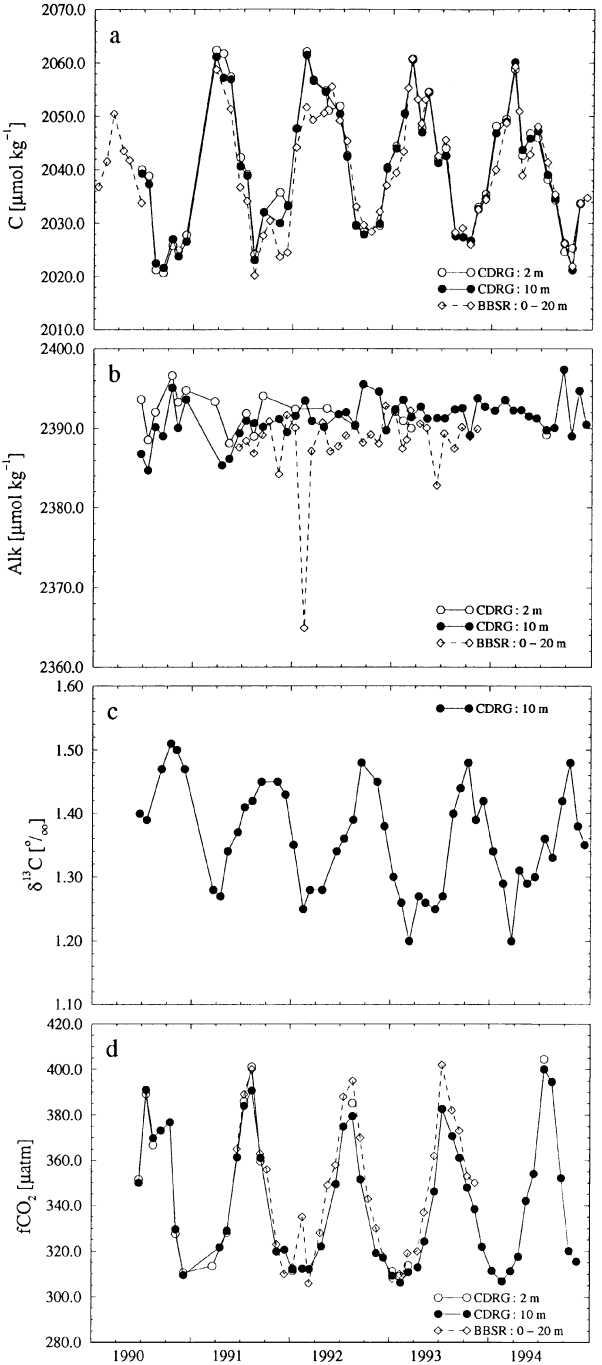
a
C [µmol kg^{-1}]
2070.0
2060.0
2050.0
2040.0
2030.0
2020.0
2010.0
CDRG : 2 m
CDRG : 10 m
BBSR : 0 – 20 m
b
Alk [µmol kg^{-1}]
2400.0
2390.0
2380.0
2370.0
2360.0
CDRG : 2 m
CDRG : 10 m
BBSR : 0 – 20 m
c
$\delta^{13}C$ [‰]
1.60
1.50
1.40
1.30
1.20
1.10
CDRG : 10 m
d
fCO_2 [µatm]
420.0
400.0
380.0
360.0
340.0
320.0
300.0
280.0
CDRG : 2 m
CDRG : 10 m
BBSR : 0 – 20 m
1990
1991
1992
1993
1994

associated with the strength of the winter-time overturning (Lueker *et al.*, 1997; Bates *et al.*, 1996b).

Normalized *Alk*, in contrast to normalized *C*, shows very little variability around an average of 2392 μmol kg^{-1} during the analysis period (Fig. 1b). Contrary to Bates *et al.* (1996a), we do not observe the sharp non-conservative decrease of *Alk* in February 1992 (BATS 41). However, the discrepancy may not be as large as suggested in Fig. 1b, because we have analyzed *Alk* only at 9 m, where the non-conservative decrease reported by Bates *et al.* (1996a) amounts to about 9 μmol kg^{-1} only. The reason for this discrepancy is unknown; similar short-time drawdowns of normalized *Alk* have also been observed at station 'S' (Lueker *et al.*, 1997).

The reduced isotopic ratio of *C*, $\delta^{13}C$, reveals a regular seasonal pattern with an amplitude of about 0.2–0.3‰ around a mean of 1.35‰ (Fig. 1c). The seasonal cycle of $\delta^{13}C$ is nearly in opposite phase to that of *C*, with minima occuring in winter/spring and maxima occurring in fall/early winter. As for *C*, this cycle of $\delta^{13}C$ at BATS is very similar to that described by Keeling (1993) and Lueker *et al.* (1997) for station 'S'. Interannual variability of $\delta^{13}C$ for the years 1990–1994 is relatively small.

The computed fugacity of CO_2 in the mixed layer, fCO_2^{oc}, exhibits a large seasonal cycle with an amplitude of over 80 μatm (Fig. 1d). It has been shown that these large seasonal fluctuations are mostly driven by the local heat balance over the year, but that the variability of *C* modifies the signal significantly in opposite direction (Keeling, 1993; Marchal, 1996; Bates *et al.*, 1996b; Lueker *et al.*, 1997). Our calculated fCO_2^{oc} values are on average about 10 μatm lower than the calculated fCO_2^{oc} reported by Bates *et al.* (1996b). This discrepancy stems mainly from the reduction of our computed fCO_2^{oc} values by 13 μatm in order to agree closely with direct fCO_2^{oc} observations during an inter-calibration cruise in the Sargasso Sea (see Appendix A and Lueker *et al.* (1997)).

3. Model description

3.1. Outline of the diagnostic model

The diagnostic model employed in our study consists of a vertically one-dimensional, box representation of the upper ocean. It is schematically shown in Fig. 2. The upper box represents the surface mixed layer (*ml*), the lower box the underlying waters of the thermocline (*tc*). The upper box exchanges CO_2 with the overlying atmosphere (*atm*) across the air–sea interface. The atmospheric and thermocline boxes are of indeterminate sizes and are included only to establish boundary conditions. The boundary between the mixed layer and the thermocline boxes is permitted to move up and down. The mixed layer dynamics are not explicitly modeled. Rather the temporal evolution of the mixed layer depth is diagnosed from observations. The concentrations of all tracers are assumed to be uniform in the mixed layer and in the atmosphere. In the thermocline, the concentrations of the tracers vary linearly with depth. Lateral advection transports water and tracers through the mixed layer box. The mixed layer therefore represents an open system with respect to all tracers.

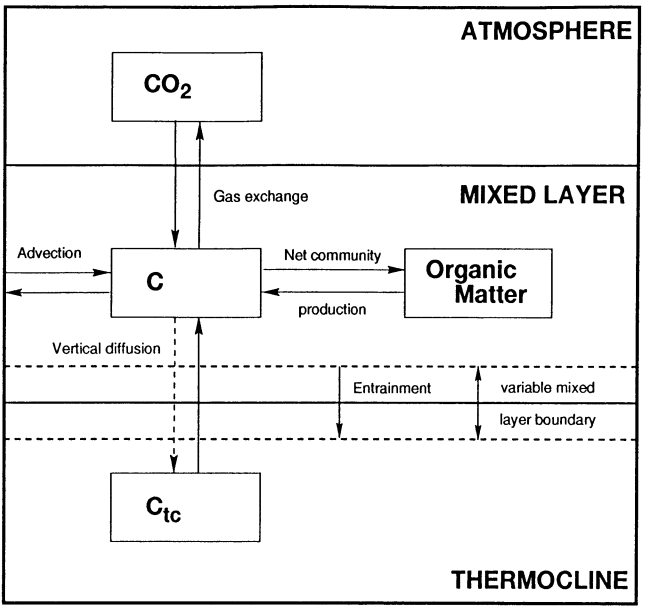

Fig. 2. Schematic representation of the one-dimensional, two box ocean model employed in the diagnostic study of the seasonal carbon cycle at station BATS near Bermuda. Dissolved inorganic carbon is explicitly modeled only in the mixed layer. The other carbon reservoirs are included only to establish boundary conditions. The depth of the mixed layer is permitted to move up and down, thereby detraining or entraining waters from the thermocline box.

The concentrations of C and ^{13}C in the mixed layer box are assumed to be affected by (1) air–sea gas exchange with the atmosphere, (2) vertical diffusion across the lower boundary, (3) entrainment of water from the thermocline whenever the mixed layer is deepening, (4) horizontal advection by the mean geostrophic flow, and (5) net transfer between inorganic and organic carbon pools (both dissolved and particulate organic carbon) due to photosynthesis and oxidiation of organic matter. We will refer to this net transfer as net community production (Williams, 1993). We do not take into account the following three processes in our carbon budget: First, we neglect the contribution of the biological production of carbonate shells. This is justified by the observed nearly conservative behaviour of alkalinity after normalization to salinity (see Fig. 1 and (Bates *et al.*, 1996b)). We do not include bloom events (Bates *et al.*, 1996a), because they have occured too infrequently. Second, we neglect Ekman convergence, because its contribution to the seasonal cycle of C has been shown to be relatively small (Michaels *et al.*, 1994). Third, we do not include the possible horizontal transport by meso-scale eddies that exist throughout the northwestern Sargasso Sea (Michaels and Knap, 1996; Siegel and Deuser, 1997), because their episodic influence is smoothed out on the seasonal time scale of our interest.

3.2. Model Equations

The temporal evolution of C (μmol kg^{-1}) in the mixed layer is thus governed by the five processes considered:

$$\frac{dC}{dt} = J_{ex} + J_{diff} + J_{ent} + J_{adv} + J_{ncp}, \tag{1}$$

$$\frac{dC}{dt} = \frac{1}{h} kL(fCO_2^{atm} - fCO_2^{oc}) + \frac{1}{h} K_z \left.\frac{dC}{dz}\right|_{tc} + \frac{1}{h} \Theta\left(\frac{dh}{dt}\right)\cdot(C_{tc} - C) - u\frac{dC}{dx} + J_{ncp}, \tag{2}$$

where J_{ex} denotes the source term due to air–sea gas exchange, J_{diff} is the source term due to vertical diffusion, J_{ent} denotes the source term due to entrainment, J_{adv} represents the source term due to advection, and J_{ncp} denotes the source term due to net community production. The variable h is the mixed layer depth (defined positively downwards), k the gas exchange velocity, L the solubility of CO_2 in seawater, fCO_2^{atm} the CO_2 fugacity in the air overlying the mixed layer, K_z the vertical diffusivity at the base of the mixed layer, $dC/dz|_{tc}$ the vertical C gradient at the base of the mixed layer, C_{tc} the C concentration in the thermocline below the mixed layer, u the mean horizontal advective velocity, and dC/dx the mean horizontal gradient of C. The units of these variables and parameters are given in Tables 1 and 2. $\Theta(dh/dt)$ is the Heaviside function, which states that shoaling of the mixed layer, $dh/dt < 0$, does not introduce new water into the mixed layer and therefore does not alter the concentration of the tracers in the mixed layer. Only the deepening of the mixed layer, $dh/dt > 0$, induces mixing with the underlying waters of the thermocline to produce changes in the tracer concentrations.

The temporal evolution of ^{13}C (μmol kg^{-1}) in the mixed layer is affected in our model by the same processes as for C ($^{12}C + {}^{13}C$):

$$\frac{d^{13}C}{dt} = {}^{13}J_{ex} + {}^{13}J_{diff} + {}^{13}J_{ent} + {}^{13}J_{adv} + {}^{13}J_{ncp}, \tag{3}$$

$$\frac{d^{13}C}{dt} = \frac{1}{h} kL \frac{\alpha_{am}}{1 + {}^{13}r_s}({}^{13}r_{atm} fCO_2^{atm} - {}^{13}r_{oc} fCO_2^{oc}\alpha_{eq}) + \frac{1}{h} K_z \left.\frac{d^{13}C}{dz}\right|_{tc} + \frac{1}{h}\Theta\left(\frac{dh}{dt}\right)({}^{13}C_{tc} - {}^{13}C) - u\frac{d^{13}C}{dx} + {}^{13}J_{ncp}, \tag{4}$$

where the $^{13}J_i$ denote the source terms for ^{13}C of the five processes considered. The parameter α_{am} is the kinetic isotopic fractionation factor for the air–sea transfer of CO_2, α_{eq} is the equilibrium isotopic fractionation factor of gaseous CO_2 with respect to C, $^{13}r_s$ is the $^{13}C/^{12}C$ ratio of the PDB standard (see Appendix A), $^{13}r_{atm}$ is the $^{13}C/^{12}C$ ratio of atmospheric CO_2, $^{13}r_{oc}$ is the $^{13}C/^{12}C$ ratio of C, $d^{13}C/dz|_{tc}$

Table 1
Definition of input variables of the seasonal diagnostic box model

Variable	Unit	Description	Source
C_{obs}	$\mu mol\,kg^{-1}$	Observed C concentration	Harmonic fit of obs.
T	°C	Mixed layer temperature	Harmonic fit of obs.
S		Mixed layer salinity[a]	Harmonic fit of obs.
h	m	Mixed layer depth	Harmonic fit of obs.
fCO_2^{oc}	µatm	Oceanic fCO_2	Harmonic fit of obs.
fCO_2^{atm}	µatm	Atmospheric fCO_2	Calc. from obs. pCO_2^{atm}
k	$m\,s^{-1}$	Gas exchange velocity	Calc. from obs. ws, T and S
ws	$m\,s^{-1}$	Wind speed	Harmonic fit of obs.
L	$\mu mol\,kg^{-1}\,\mu atm^{-1}$	CO_2 solubility in sea water	Calc. from obs. T and S
$dC/dz\|_{tc}$	$\mu mol\,kg^{-1}\,m^{-1}$	Vertical C gradient	Harmonic fit of obs.
$d^{13}C/dz\|_{tc}$	$\mu mol\,kg^{-1}\,m^{-1}$	Vertical ^{13}C gradient	Calc. from obs. $dC/dz\|_{tc}$ and $d\delta^{13}C/dC\|_{tc}$
K_z	$m^2\,s^{-1}$	Vertical diffusion coefficient at the base of the mixed layer	Calc. from the buoyancy frequency
C_{tc}	$\mu mol\,kg^{-1}$	C conc. in the thermocline box	Calc. from l_{ent} and $dC/dz\|_{tc}$
$^{13}r_{oc}$		$^{13}C/^{12}C$ ratio of C	Calc. from obs. $\delta^{13}C$
$^{13}r_{atm}$		$^{13}C/^{12}C$ ratio of atm. CO_2	Calc. from obs. $\delta^{13}C_{atm}$
α_{eq}		Equilibrium isotopic fractionation factor of gaseous CO_2 with respect to C	Calc. from T
$^{13}C_{tc}$	$\mu mol\,kg^{-1}$	^{13}C conc. in the thermocline box	Calc. from l_{ent}, $dC/dz\|_{tc}$ and $d\delta^{13}C/dC\|_{tc}$
$d^{13}C/dx$	$\mu mol\,kg^{-1}\,m^{-1}$	Horizontal ^{13}C gradient	Calc. from dC/dx and $d\delta^{13}C/dx$
$^{13}r_{org}$		$^{13}C/^{12}C$ ratio of organic matter	Calc. from fCO_2^{oc}, T and S

[a] To conform to UNESCO (1981) no unit is shown.

Table 2
Definition and standard values of parameters of the seasonal diagnostic box model

Parameter	Value	Unit	Description
ρ_0	1026.2	$kg\,m^{-3}$	Average density of sea water
$^{13}r_s$	0.0112372		$^{13}C/^{12}C$ ratio of PDB standard
α_{am}	0.99820		Kinetic isotopic fractionation factor for the air–sea transfer of CO_2
$d\delta^{13}C/dC\|_{tc}$	–0.0052	$‰\,\mu mol^{-1}\,kg$	Ratio of vertical $\delta^{13}C$ and C gradient in the thermocline
l_{ent}	12	m	Length scale of entrainemt
u	–0.05	$m\,s^{-1}$	Mean horizontal velocity
dC/dx	1.1×10^{-5}	$\mu mol\,kg^{-1}\,m^{-1}$	Mean horizontal C gradient
$d\delta^{13}C/dx$	-1.2×10^{-7}	$‰\,m^{-1}$	Mean horizontal $\delta^{13}C$ gradient

is the ^{13}C gradient at the base of the mixed layer, $^{13}C_{tc}$ the ^{13}C concentration in the thermocline below the mixed layer, and $d^{13}C/dx$ is the mean horizontal gradient of ^{13}C. The units of these variables and parameters are given in Tables 1 and 2.

The source term of net community production (J_{ncp}) is related to the corresponding ^{13}C source term ($^{13}J_{ncp}$) by the $^{13}C/^{12}C$ ratio of organic matter, $^{13}r_{org}$:

$$J_{ncp} = \frac{1 + {}^{13}r_{org}}{{}^{13}r_{org}} \; {}^{13}J_{ncp}. \tag{5}$$

We now solve Eq. (4) for $^{13}J_{ncp}$, assuming that we know $\mathrm{d}^{13}C/\mathrm{d}t$ from the observations, and insert the result into Eq. (2) by using Eq. (5). This yields:

$$\frac{\mathrm{d}C}{\mathrm{d}t} = J_{phys} + \frac{1 + {}^{13}r_{org}}{{}^{13}r_{org}} \left(\left. \frac{\mathrm{d}^{13}C}{\mathrm{d}t} \right|_{obs} - {}^{13}J_{phys} \right), \tag{6}$$

where we have introduced J_{phys} and $^{13}J_{phys}$, which represent the sum of the source terms of air–sea gas exchange, vertical diffusion, entrainment and advection.

Next we need to replace ^{13}C in Eq. (6) by an expression based on $^{13}r_{oc}$, because the variability of ^{13}C is for the most part determined by the variability in C and to a far lesser extent by the variability in $^{13}r_{oc}$. If we calculated $\mathrm{d}^{13}C/\mathrm{d}t\,|_{obs}$ from the $\delta^{13}C$ and C observations and inserted it into Eq. (6), we would force the simulated $\mathrm{d}C/\mathrm{d}t$ very strongly towards the observed $\mathrm{d}C/\mathrm{d}t\,|_{obs}$. To avoid this, we replace ^{13}C by $^{13}r_{oc}\; C/(1 + {}^{13}r_{oc})$ and get:

$$\frac{\mathrm{d}C}{\mathrm{d}t} = J_{phys} + \frac{1 + {}^{13}r_{org}}{{}^{13}r_{org}} \left(\frac{C}{(1 + {}^{13}r_{oc})^2} \frac{\mathrm{d}^{13}r_{oc}}{\mathrm{d}t} + \frac{{}^{13}r_{oc}}{1 + {}^{13}r_{oc}} \frac{\mathrm{d}C}{\mathrm{d}t} - {}^{13}J_{phys} \right). \tag{7}$$

The reason for this replacement is now more evident, because the expression $\mathrm{d}C/\mathrm{d}t$ can be found on both sides of Eq. (7). We solve Eq. (7) for $\mathrm{d}C/\mathrm{d}t$ to obtain the final equation of the diagnostic model:

$$\begin{aligned} \frac{\mathrm{d}C}{\mathrm{d}t} = {} & \frac{{}^{13}r_{org}(1 + {}^{13}r_{oc})}{{}^{13}r_{org} - {}^{13}r_{oc}} J_{phys} + \frac{1 + {}^{13}r_{org}}{(1 + {}^{13}r_{oc})({}^{13}r_{org} - {}^{13}r_{oc})} C \frac{\mathrm{d}^{13}r_{oc}}{\mathrm{d}t} \\ & - \frac{(1 + {}^{13}r_{oc})(1 + {}^{13}r_{org})}{{}^{13}r_{org} - {}^{13}r_{oc}} {}^{13}J_{phys}. \end{aligned} \tag{8}$$

We can thus compute the temporal evolution of C in the mixed layer from the observed change in the $^{13}C/^{12}C$ ratio of C and independent estimates of the contribution of the physical processes (J_{phys} and $^{13}J_{phys}$). The computed evolution of C can then be compared to the observed variability of C to check the consistency of the calculations.

The magnitude of net community production is calculated by difference:

$$J_{ncp} = \frac{\mathrm{d}C}{\mathrm{d}t} - J_{phys}. \tag{9}$$

3.3. Integrated fluxes and source terms

In order to establish the carbon budget of the mixed layer over different periods of the year, we calculate temporally integrated fluxes and source terms of the different

processes considered. The temporally integrated source term of process i between time t_0 and t (denoted by $\mathcal{J}_i$) is calculated as:

$$\mathcal{J}_i = \int_{t_0}^{t} J_i \, \mathrm{d}t, \tag{10}$$

and has units of $\mu\mathrm{mol\,kg^{-1}}$. The corresponding temporally integrated flux (denoted by $\mathcal{F}_i$) is given by

$$\mathcal{F}_i = \rho_0 \int_{t_0}^{t} h J_i \, \mathrm{d}t, \tag{11}$$

and has units of $\mathrm{mol\,m^{-2}}$. As a check of the consistency of the simulation, we compare the simulated $\mathcal{J}_{\mathrm{sim}}$ and $\mathcal{F}_{\mathrm{sim}}$ (sum of all considered processes) with the observed $\mathcal{J}_{\mathrm{obs}}$ and $\mathcal{F}_{\mathrm{obs}}$ based on direct observations:

$$\mathcal{J}_{\mathrm{obs}} = \int_{t_0}^{t} \left.\frac{\mathrm{d}C}{\mathrm{d}t}\right|_{\mathrm{obs}} \mathrm{d}t = (C_{\mathrm{obs}}(t) - C_{\mathrm{obs}}(t_0)), \tag{12}$$

$$\mathcal{F}_{\mathrm{obs}} = \rho_0 \int_{t_0}^{t} h \left.\frac{\mathrm{d}C}{\mathrm{d}t}\right|_{\mathrm{obs}} \mathrm{d}t. \tag{13}$$

Note that $\mathcal{F}_{\mathrm{obs}}$ over the annual cycle is not zero, even when the seasonal cycle of C is stationary, because of a small covariance of the seasonal variability of h and $\mathrm{d}C/\mathrm{d}t|_{\mathrm{obs}}$. In order to close the mixed layer budget with respect to the temporally integrated fluxes, we have to evaluate the total mass flux of carbon, $\mathcal{F}_{\mathrm{tot}}$:

$$\mathcal{F}_{\mathrm{tot}} = \rho_0 \int_{t_0}^{t} \frac{\mathrm{d}(hC)}{\mathrm{d}t} \mathrm{d}t = \mathcal{F}_{\mathrm{obs}} + \rho_0 \int_{t_0}^{t} C \frac{\mathrm{d}h}{\mathrm{d}t} \mathrm{d}t, \tag{14}$$

where we calculate the contribution of the second term on the right-hand side of Eq. (14) diagnostically from the observed variability of C and h.

3.4. Determination of model input variables and parameters

We must restrict our diagnostic model analysis of the seasonal carbon cycle in the mixed layer to the four years from 1991 to 1994, because there are no carbon measurements available from BBSR for 1990 (Bates *et al.*, 1996a, b). Those are needed in our analysis to establish vertical boundary conditions (see below). In addition to the CDRG carbon observations, we use physical and chemical data from the hydrographic core measurements made at BATS for the same period (Knap *et al.*, 1993, 1994; Michaels and Knap, 1996).

We drive our model with smooth forcing functions created by combining the time series of each input variable into a composite one-year sequence without regard to interannual variability. Thus the model provides a "climatological" average for the period 1991–1994. A harmonic function of the form

$$H = \sum_{k=1}^{m} \left[a_k \sin\left(\frac{2\pi k t}{365}\right) + b_k \cos\left(\frac{2\pi k t}{365}\right) \right] + H_0 \tag{15}$$

is fitted by a least-squares method to the annual composite data. In Eq. (15), a_k, b_k and H_0 represent constants that are specific for each variable; t denotes the time in days. The number of retained harmonics in our analysis depends on the significance of the parameters a_k and b_k inferred from a Students-t test (Bronstein and Semendjajew, 1989) (p. 681) at the 95% confidence level. The obtained parameters of all fits, including the coefficient of correlation, R^2, are given in Table 3. In the next sections, we describe in detail the model variables and parameters used in our model study. A summary of them is given in Tables 1 and 2.

3.4.1. Carbon and general input variables

Fig. 3 shows the time series data of C, $\delta^{13}C$ and calculated fCO_2^{oc}, composited over the annual cycle, together with their harmonic representations. C and $\delta^{13}C$ are nearly in opposite phase with the extrema occuring around March/April and September/October, respectively. fCO_2^{oc} exhibits relatively constant values around 310 µatm in winter and early spring and a sharp maximum in summer with values attaining 400 µatm.

Mixed layer temperature (T) and salinity (S) were determined by calculating the averages of all observations in the upper 20 m. Mixed layer temperature (Fig. 4a) has a distinct seasonal pattern with minimum temperatures of slightly less than 20°C in March/April and maximum temperatures above 28°C in August. Mixed layer salinity (Fig. 4b) shows a weak seasonal pattern with a maximum of about 36.65 during the winter/spring period and a minimum of about 36.50 during late summer/fall, when precipitation exceeds evaporation (Siegel *et al.*, 1995; Doney *et al.*, 1996). We estimated the vertical extent of the surface mixed layer (h) based on all available CTD casts by applying a constant $\Delta\sigma_t$ criterion of 0.125 kg m^{-3} between the mean density of the surface top 10 m and the density at base of the mixed layer (Levitus, 1982). We tested also the variable σ_θ criterion of Sprintall and Tomczak (1992) with a temperature difference of 0.5°C and found almost identical mixed layer depths (mean difference to Levitus criterion of -2 ± 4 m). All casts on a particular occupation of

Table 3
Harmonic fitting coefficients of Eq. (15)

Parameter	Unit	H_0	a_1	b_1	a_2	b_2	a_3	b_3	R^2
C_{obs}	µmol kg^{-1}	2042.1	15.56	1.00	0.55	0.25			0.88
$\delta^{13}C$	‰	1.350	−0.101	0.008					0.81
$\delta^{13}C_{atm}$	‰	−7.875	−0.238	−0.078	0.109	−0.038			0.96
fCO_2^{oc}	µatm	346.44	−20.56	−27.03	8.25	6.67			0.95
pCO_2^{atm}	ppm	356.89	4.35	1.13	−2.00	0.76	0.40	−0.36	0.98
T	°C	23.51	−3.20	−2.43	0.60	0.47			0.96
S		36.587	0.085	0.027					0.29
h	m	74.82	43.68	55.98	21.76	−9.66	−0.33	−7.66	0.65
ws	m s^{-1}	7.17	0.76	1.89	0.06	−0.28			0.98
$dC/dz\|_{tc}$	µmol kg^{-1} m^{-1}	0.51	−0.16	0.17					0.57
K_z	10^{-4} m^2 s^{-1}	0.362	0.431	0.090	0.054	−0.191	−0.076	0.009	0.76

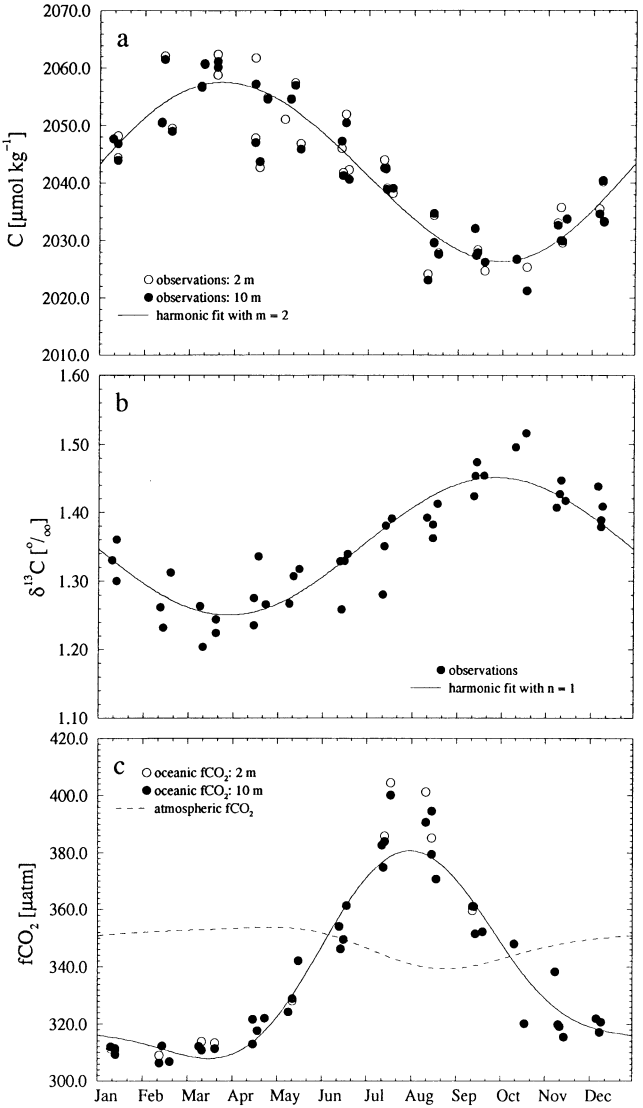

Fig. 3. Annual composite time series (a) of C (µmol kg^{-1}), (b) of $\delta^{13}C$ (‰), and (c) of calculated fCO_2^{oc} (µatm) at the (BATS station for the years 1991–1994. The circles represent the observations, whereas the smooth curve represents the results of the harmonic fit through the observations (see Eq. (15)). Also shown in (c) is the estimated fCO_2^{atm} (µatm) near Bermuda, which has been calculated using the mean atmospheric pressure and relative humidity observed at St. Davids Head on the island of Bermuda (Knap *et al.*, 1992; Knap *et al.*, 1993) and observations of the CO_2 mixing ratio at La Jolla, California (Lueker *et al.*, 1997). This station is at nearly the same latitude as Bermuda and has a very similar seasonal cycle of atmospheric CO_2 as the Bermuda East station.

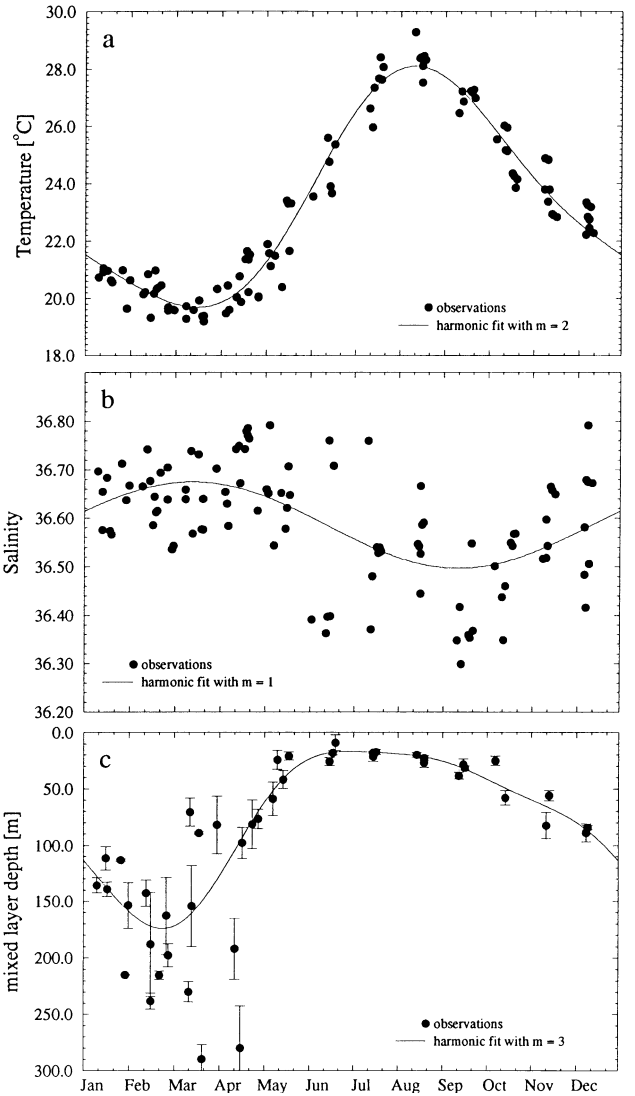

Fig. 4. Annual composite time series (a) of mixed layer temperature (°C), (b) of mixed layer salinity, and (c) of the estimated mixed layer depth (m) at the BATS station for the years 1991–1994. The circles represent the observations, whereas the smooth curve represents the results of the harmonic fit through the observations (see Eq. (15)). Mixed layer temperature and salinity have been calculated by averaging the observations in the upper 20 m. The mixed layer depth was estimated from CTD data by using a constant $\Delta\sigma_t$ criterion of 0.125 kg m^{-3} (see text). The circles denote the average of all CTD casts during a particular station occupation and the error bar the standard deviation.

the BATS site were averaged. The thickness of the surface mixed layer shows a large seasonal variability mainly caused by the large seasonal changes in the heat exchange and wind stress at the surface (Musgrave *et al.*, 1988; Doney *et al.*, 1996). Maximum mixed layer depths are found in late winter/early spring with depths ranging from 150 to 300 m. Afterwards the layer shoals, but the transition is highly erratic owing to intermittent convective events and restratification acting on a weak vertical density gradient. In June, a stable shallow mixed layer of about 20 m is established, which lasts until beginning of August. Then the layer gradually deepens as a result of cooling and increased wind stress until the time of maximum vertical overturning in February/March.

3.4.2. Air–sea gas exchange

The CO_2 fugacity in the atmosphere, fCO_2^{atm}, is calculated from the CO_2 mixing ratio in the atmosphere recorded at La Jolla, California, at 32.9°N on the Pacific coast of North America. We chose this station because this is the only site at approximately the same latitude where concurrent observations of the atmospheric $^{13}C/^{12}C$ ratio are available for the investigated period. Because the seasonal cycle in the atmospheric CO_2 mixing ratio varies only slightly with longitude in mid-latitudes (Heimann *et al.*, 1989), we deem the data for La Jolla to be adequate. This has been verified for the years 1989 to 1992 with data obtained at the Station Bermuda East (WMO/WDCGG, 1995). To convert the CO_2 mixing ratios into CO_2 fugacities we have used the annual mean surface pressure of 1.017 atm and the annual mean relative humidity of 0.87 observed at St. David's head on Bermuda (Knap *et al.*, 1992, 1993). We used seasonal mean quantities because neither surface pressure nor relative humidity show significant seasonal variations (Marchal, 1996). However, they both vary strongly on the atmospheric synoptic time-scale. We neglect these variations of pressure and relative humidity, because their standard deviation of 0.006 atm for pressure and 0.06 for relative humidity add an uncertainty of only about 2 μatm to the computed fCO_2^{atm}, considerably smaller than the uncertainty that we associate with the computed fCO_2^{oc} (10 μatm). The $^{13}C/^{12}C$ ratio in the atmosphere, $\delta^{13}r_{atm}$ is calculated from the harmonic representation of the $\delta^{13}C_{atm}$ observations at La Jolla shown in Fig. 5a.

The CO_2 solubility in sea water, L, is computed from T and S using the solubility of Weiss (1974). We adopt the relationship proposed by Wanninkhof (1992) for long term averaged winds for the wind speed ependency of the gas exchange velocity, k. The Schmidt number for CO_2 was calculated from T according to the polynomial function of Wanninkhof (1992). Monthly average wind speed data (shown in Fig. 5b) were taken from Isemer and Hasse (1985) and also fitted with a harmonic function (15). The parameter α_{am}, the kinetic $^{13}C/^{12}C$ fractionation factor for the CO_2 uptake by the surface ocean, is assumed to be constant with a value of 0.99820 (Keeling *et al.*, 1989) (p. 189). We approximate the equilibrium $^{13}C/^{12}C$ fractionation factor of gaseous CO_2 with respect to C by the directly measured fractionation factor of gaseous CO_2 with respect to HCO_3^-, $\alpha_{eq} \approx \alpha_b = 1.02389 - 9.483\ \mathrm{K}/(T + 273.15\ \mathrm{K})$ (Mook *et al.*, 1974). This approximation is justified because dissolved inorganic carbon consists of about 85% HCO_3^-, and the fractionation factors for the remaining inorganic carbon species are nearly the same as for HCO_3^-.

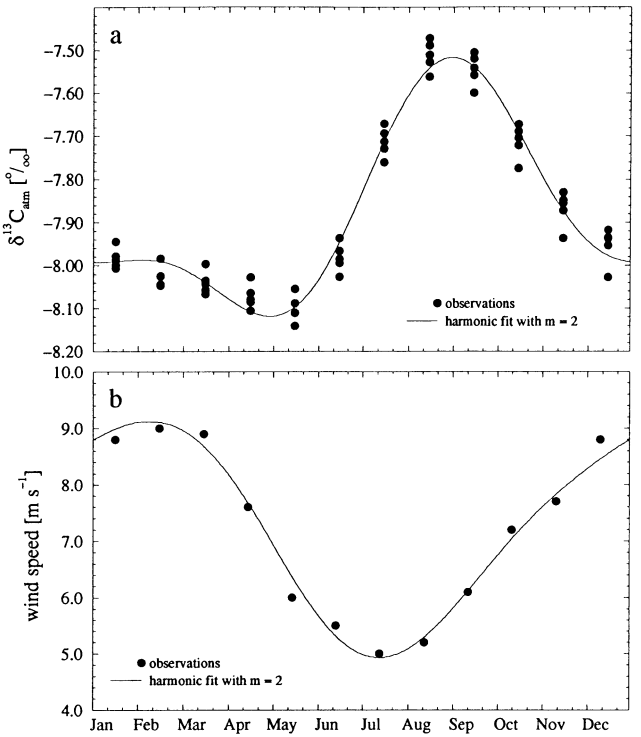

Fig. 5. Annual composite time series of input variables at the sea-surface. (a) Plot of the reduced $^{13}C/^{12}C$ ratio in the atmosphere, $\delta^{13}C_{atm}$ in ‰, observed at La Jolla, California, from 1991 to 1994. The circles denote the linearly detrended monthly mean values and the smooth curve the result of the harmonic fit through the data (see Eq. (15)). (b) Climatological monthly mean wind speed data from Isemer and Hasse (1985) (circles) (m s^{-1}) and harmonic fit through these data (smooth curve).

3.4.3. *Vertical diffusion*

We estimated the vertical C gradient below the mixed layer, $dC/dz|_{tc}$, from the BBSR observations of C for the investigated period. After the average mixed layer depth of the station had been estimated from the CTD data, $dC/dz|_{tc}$ was determined by fitting a linear regression to the C observations in the 50 m deep water column directly underneath the base of the mixed layer. The vertical C gradient (Fig. 6a) is relatively small (0.2 μmol kg^{-1} m^{-1}) in spring and early summer, but increases steadily to about 0.7 μmol kg^{-1} m^{-1} in fall and winter. The annual average of 0.51 μmol kg^{-1} m^{-1} is close to the estimated mean $dC/dz|_{tc}$ of 0.45 μmol kg^{-1} m^{-1} at station 'S' (Gruber and Keeling, 1998). We lack corresponding $\delta^{13}C$ data at BATS to determine the vertical ^{13}C gradient at the base of the mixed layer, $d^{13}C/dz|_{tc}$. However, C and $\delta^{13}C$ are relatively well correlated in the thermocline of the North Atlantic. Fig. 7 shows a plot of C versus $\delta^{13}C$ in the thermocline between 100 and 700 m based on four profiles taken at station 'S' between 1984 and 1990 (Lueker *et al.*, 1997) and eight nearby stations from the Transient Tracer in the Oceans North Atlantic Study (TTO NAS) in 1981 (C.D. Keeling, unpublished measurements). Linear regression of these

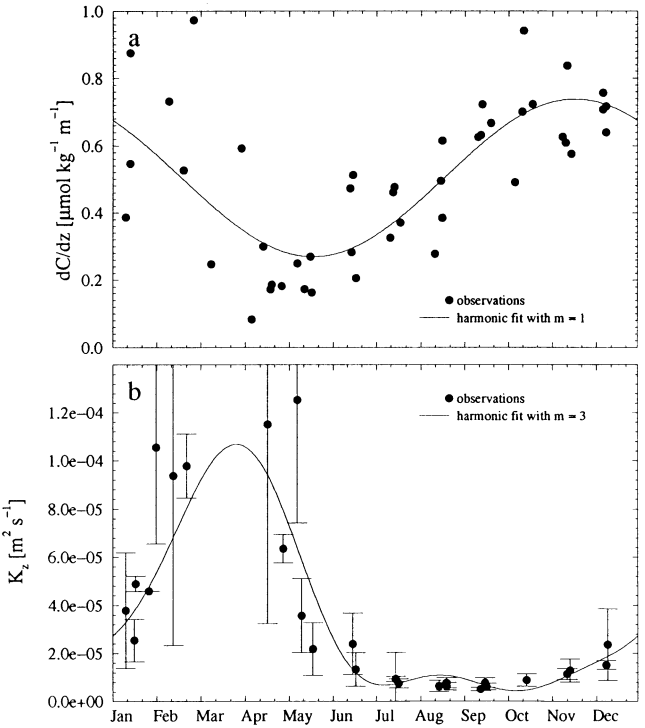

Fig. 6. Annual composite time series of input variables at the lower boundary of the mixed layer. (a) Plot of the vertical C gradient at the base of the mixed layer $\mathrm{d}C/\mathrm{d}z|_{\mathrm{tc}}$ in µmol kg^{-1} m^{-1} for the years 1991–1994. The circles denote the observations, which have been estimated by a linear regression to the C data points in the first 50 m of the column underlying the mixed layer. The smooth line represents the result of the harmonic fit (see Eq. (15)). (b) Annual composite time series of the vertical diffusion coefficient in m^2 s^{-1} at the base of the mixed layer from 1991 to 1994, computed from the local buoyancy frequency determined from CTD data using Eq. (17) (see text). The circles denote the average of all K_z determinations on a particular station occupation and the error bar the standard deviation. Stations where no clear mixed layer was discernible have been omitted from the analysis.

data yields a slope $\mathrm{d}\delta^{13}C/\mathrm{d}C|_{\mathrm{tc}}$ of $-0.0052 \pm 0.0004‰$ µmol^{-1} kg ($R^2 = 0.92$). This slope is in good agreement with the slope of $-0.0047‰$ µmol^{-1} kg determined by Gruber and Keeling (1998) based on observations directly underneath the mixed layer at Station 'S' and the results of a three-dimensional ocean general circulation model (Bacastow and Maier-Reimer, 1991). The investigated depth range is much greater than the depth range of interest directly below the mixed layer. To take this uncertainty into account, we subjectively assign to $\mathrm{d}\delta^{13}C/\mathrm{d}C|_{\mathrm{tc}}$ an uncertainty of twice the standard deviation. In our model, the vertical ^{13}C gradient below the mixed layer $\mathrm{d}^{13}C/\mathrm{d}z|_{\mathrm{tc}}$ is then computed from $\mathrm{d}\delta^{13}C/\mathrm{d}C|_{\mathrm{tc}}$, the vertical C gradient, and the mixed layer C and $\delta^{13}C$ by

$$\left.\frac{\mathrm{d}^{13}C}{\mathrm{d}z}\right|_{\mathrm{tc}} = \frac{{}^{13}r_{\mathrm{s}}(\delta^{13}C + 1)}{1 + {}^{13}r_{\mathrm{s}}\delta^{13}C + {}^{13}r_{\mathrm{s}}} \left.\frac{\mathrm{d}C}{\mathrm{d}z}\right|_{\mathrm{tc}} + \frac{{}^{13}r_{\mathrm{s}}\, C}{(1 + {}^{13}r_{\mathrm{s}}\delta^{13}C + {}^{13}r_{\mathrm{s}})^2} \left.\frac{\mathrm{d}\delta^{13}C}{\mathrm{d}z}\right|_{\mathrm{tc}}. \qquad (16)$$

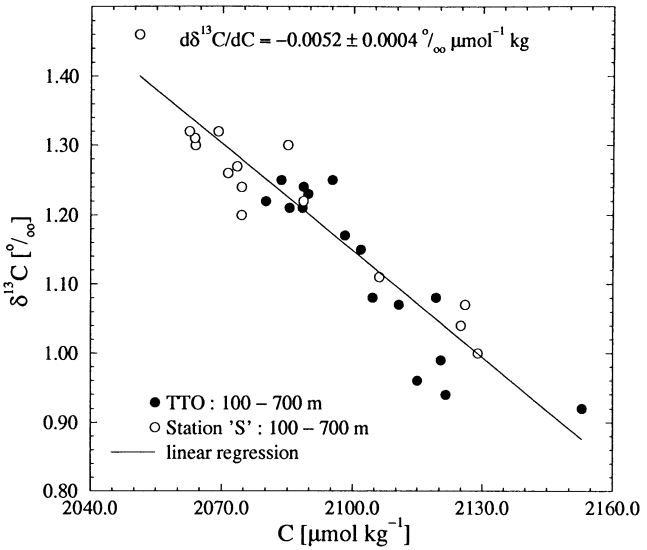

Fig. 7. Plot of $\delta^{13}C$ versus C in the main thermocline of the subtropical North Atlantic between 100 and 700 m depth. The data are from 4 vertical profiles taken at station 'S' between 1984 and 1990 (Lueker *et al.*, 1997) and from eight nearby stations from the Transient Tracer in the Oceans North Atlantic Study (TTO NAS) in 1981 (C.D. Keeling, unpublished measurements). A linear regression analysis of these data gives a slope of $-0.0052 \pm 0.0004‰\ \mu mol^{-1}\ kg$ ($R^2 = 0.92$).

The vertical diffusion coefficient at the base of the mixed layer was determined according to the formula of Denman and Gargett (1983):

$$K_z = 0.25\varepsilon N^{-2}, \tag{17}$$

where ε denotes the rate of turbulent energy dissipation, assumed to be constant, and N is the Brunt Väisälä frequency. Following Oudot (1989), we have chosen ε to be equal to $2.0 \times 10^{-8}\ m^2\ s^{-3}$, a value that seems representative of the upper ocean thermocline at times of low wind speeds (Dillon and Caldwell, 1980) (p. 257). N was computed from the vertical density gradient at the base of the mixed layer, estimated by a linear regression to all CTD observations in the 20 m deep water column underlying the base of the mixed layer. Occasions where no distinct mixed layer was detectable were omitted. To construct the composite time series shown in Fig. 6b, all K_z determinations during a particular station occupation were averaged and the standard deviation computed. We find a large seasonal variability for K_z, with values around $1.0 \times 10^{-4}\ m^2\ s^{-1}$ in winter and early spring, when the mixed layer is deepest, and low and nearly constant values around $1.0 \times 10^{-5}\ m^2\ s^{-1}$ throughout the summer/fall period. The summer/fall values agree well with estimates based on microstructure measurements (Denman and Gargett, 1983; Gregg, 1987) and on an open ocean tracer release experiment (Ledwell *et al.*, 1993), both obtained in the main thermocline. Our winter values are almost an order of magnitude greater, but they still

lie within the range of estimates based on bulk mixed-layer models for the Bermuda area (Musgrave *et al.*, 1988; Doney *et al.*, 1996) and on observations during the passage of a storm in the North Pacific (Large *et al.*, 1986).

3.4.4. Entrainment

We estimate the C and ^{13}C concentrations in the thermocline below the mixed layer, C_{tc} and $^{13}C_{tc}$, by

$$C_{tc} = C + l_{ent} \left. \frac{dC}{dz} \right|_{tc}, \tag{18}$$

$$^{13}C_{tc} = {}^{13}C + l_{ent} \left. \frac{d^{13}C}{dz} \right|_{tc}, \tag{19}$$

where l_{ent} denotes the entrainment length scale. This parameter can be thought of as representing the thickness of the layer underneath the mixed layer that is affected by the short-time variability of the mixed layer depth, caused for example, by intermittent convective events, by restratification or by the passage of internal waves. We use for l_{ent} a value of 12 m, the mean short-time variability of the mixed layer depth observed at BATS during the approximately three days occupations (see Fig. 4c). However, we must acknowledge that the value of this parameter is physically poorly constrained and that it reflects a peculiarity of the box model representation of the mixed layer. Matear (1995), for example, used $l_{ent} = 1$ m, whereas Hurtt and Armstrong (1996) replaced l_{ent} by the mixed layer depth h. We take this large uncertainty into account by subjectively assigning a large uncertainty of ± 6 m ($\pm$ 50%) to l_{ent}.

3.4.5. Horizontal advection

We chose a value of $-0.05\ m\ s^{-1}$ (x defined positively northwards) for the horizontal advective velocity u. This value is based on the estimates of Siegel and Deuser (1997) (current meter data) and Olbers *et al.* (1985) (geostrophic flow constrained by climatological hydrography in the North Atlantic). The uncertainty of this estimate is large, and therefore an uncertainty of $\pm 0.05\ m\ s^{-1}$ is given to u. Bates *et al.* (1996b) measured the horizontal C gradient on a series of seasonal meridional cruises between 27.5°N and 34.5°N along 64°W. They found that C increases in the south-to-north direction by 5–10 $\mu mol\ kg^{-1}$ over distances of approximately 700 km. We therefore assume $dC/dx = (1.1 \pm 0.3) \times 10^{-5} \mu mol\ kg^{-1}\ m^{-1}$. The horizontal gradient of $\delta^{13}C$ is estimated to be about $(-1.2 \pm 1.2) \times 10^{-7}‰\ m^{-1}$ based on measurements obtained by CDRG during the TTO North Atlantic and Tropical Atlantic cruises in 1981 and 1982/1983 (Gruber, 1997). A similar meridional gradient for $\delta^{13}C$ can be deduced from the North Atlantic data reported by Lynch-Stieglitz *et al.* (1995). In analogy to Eq. (16), the horizontal gradient for ^{13}C, $d^{13}C/dx$, is calculated from $d\delta^{13}C/dx$, dC/dx and the mixed layer C and $\delta^{13}C$ by,

$$\frac{d^{13}C}{dx} = \frac{{}^{13}r_s(\delta^{13}C + 1)}{1 + {}^{13}r_s\delta^{13}C + {}^{13}r_s} \frac{dC}{dx} + \frac{{}^{13}r_s C}{(1 + {}^{13}r_s\delta^{13}C + {}^{13}r_s)^2} \frac{d\delta^{13}C}{dx}. \tag{20}$$

3.4.6. Net community production

We calculate the $^{13}C/^{12}C$ ratio of organic matter, $^{13}r_{org}$, from the $\delta^{13}C$ of organic matter, evaluated according to the formula of Rau *et al.* (1989). They related the observed variability in $\delta^{13}C$ of plankton to differences in CO_2 solubility, based mainly on data from the South Atlantic and Southern Oceans and found empirically that

$$\delta^{13}C_{org} = (-0.8\ \mathrm{kg\,\mu mol^{-1}}\ [CO_2(aq)] - 12.6)10^{-3}, \tag{21}$$

where $[CO_2(aq)]$ denotes the local concentration of dissolved CO_2 in seawater in $\mu mol\,kg^{-1}$, computed from fCO_2^{sc} and the CO_2 solubility, L. Because the seasonal variability of $CO_2(aq)$ is small at BATS, $\delta^{13}C_{org}$ is found to vary over only a narrow range ($\pm 0.5‰$) from its average of $-20.7‰$. Druffel *et al.* (1992) measured $\delta^{13}C$ of organic matter very close to the BATS site (31°50′N, 63°30′W) in May/June 1989. They found an average $\delta^{13}C$ of particulate and dissolved organic carbon in the top 100 m of $-20.8 \pm 0.5‰$ and $-21.2 \pm 0.2‰$. These values agree well with our computed $\delta^{13}C_{org}$ of $-20.9‰$ for these two months.

3.5. Numerical implementation

The linear first-order differential equation of the diagnostic model (8) is solved using the Euler method (Press *et al.*, 1992). This method is accurate only to first order in time, but testing of the numerical scheme by backward integration showed that this is sufficient. The simulations are run for one year, starting on the first of January with a constant time step of one day. The harmonic representation of the observed C concentration for this day is used as the initial concentration.

3.6. Evaluating uncertainties with a Monte Carlo analysis

The results of the seasonal diagnostic box model are all influenced to some degree by the uncertainties of the model parameters. We assess the uncertainties in the model results with Monte Carlo simulations (Rubinstein, 1981). The errors computed with the Monte Carlo method are a function of the uncertainties assigned to the model parameters. Details of the Monte Carlo simulations are given in Appendix B.

4. Model results and discussion

4.1. Seasonal patterns

The seasonal variability of the computed source terms of the five processes given in Eq. (1), J_i, are shown in Fig. 8a and b together with the standard deviations evaluated by the Monte Carlo analysis. Substantial variations are exhibited by air–sea gas exchange, entrainment and net community production. Seasonal variations are smaller for vertical diffusion. The contribution of advection is constant over the year due to our choice of constant horizontal velocity, u, and gradients (dC/dx and $d\delta^{13}C/dx$).

The contribution of air–sea gas exchange (Fig. 8a) is positive (i.e. net uptake) with a more or less constant rate of approximately 0.08 ± 0.03 μmol kg^{-1} d^{-1} from mid-November to mid-May. This nearly constant rate is due to balancing effects of the variability in the gas exchange velocity, in the mixed layer depth and in the CO_2 fugacity difference between the atmosphere and the ocean. In winter, during the time of maximum difference in air–sea CO_2 fugacity and in gas exchange velocity, the mixed layer is deep, and therefore the input due to air–sea gas exchange is distributed over a large volume. In early summer, both the fCO_2 difference across the air-sea interface and the gas exchange velocity are small, but the mixed layer is also shallow, therefore resulting in almost the same rate of gas exchange as in winter. Starting at the beginning of May, surface warming forces fCO_2^{oc} above fCO_2^{atm}. The ocean loses CO_2 to the atmosphere during the entire summer, with a maximum rate of about -0.13 ± 0.03 μmol kg^{-1} d^{-1}.

The source term of vertical diffusion is found to be small (0.006–0.030 μmol kg^{-1} d^{-1}) throughout the year, with an uncertainty of approximately 0.02 μmol kg^{-1} d^{-1}. The source term of entrainment is zero from the end of February until the end of June, since the mixed layer depth shoals during this period ($\Theta(dh/dt) = 0$). After the beginning of August, the contribution of entrainment becomes rapidly larger, with a maximum of 0.13 μmol kg^{-1} d^{-1} in mid September, when both the rate of change in mixed layer depth, dh/dt, and the vertical C gradient at the base of the mixed layer, $dC/dz|_{tc}$, are large. Uncertainties associated with the entrainment are relatively large (up to 0.10 μmol kg^{-1} d^{-1}), especially when the contribution of this process is near the maximum. Advection adds C at a constant rate of 0.05 ± 0.03 μmol kg^{-1} d^{-1} to the mixed layer.

Net community production removes C from the mixed layer during almost the entire year (positive net community production). The maximum net community production is found at the beginning of June, where the rate attains -0.31 ± 0.04 μmol kg^{-1} d^{-1}. This maximum occurs at least one to two months later than the maximum in net primary production (spring bloom), which is usually observed in February to April (Lohrenz *et al.*, 1992; Michaels *et al.*, 1994a, b; Michaels and Knap, 1996). This need not represent a discrepancy, since the temporal variability of net community and net primary production can be decoupled. However, interpretation of this time lag must be done cautiously, since the exact timing of the maximum of net community production in the diagnostic model strongly depends on the shape of the curve describing the observed $\delta^{13}C$ variability. For $\delta^{13}C$, we used a harmonic fit with only the period of 12 months, because the data from the three years of observations did not justify the inclusion of shorter periods on the basis of a Students-t test. Therefore any existing variability on time scales shorter than twelve months is not resolved. Additionally, the shape of the input function for the mixed layer depth also influences the exact timing and magnitude of the maximum in net community production (Gruber and Keeling, 1998).

Fig. 8c depicts the sum of all simulated source terms (sum of the five curves shown in Fig. 8a and b, J_{sim}) in comparison with the observed source term J_{obs}, calculated from the harmonic representation of C. In general, good agreement between the two curves is found. The standard deviation of the simulated curve, determined from the

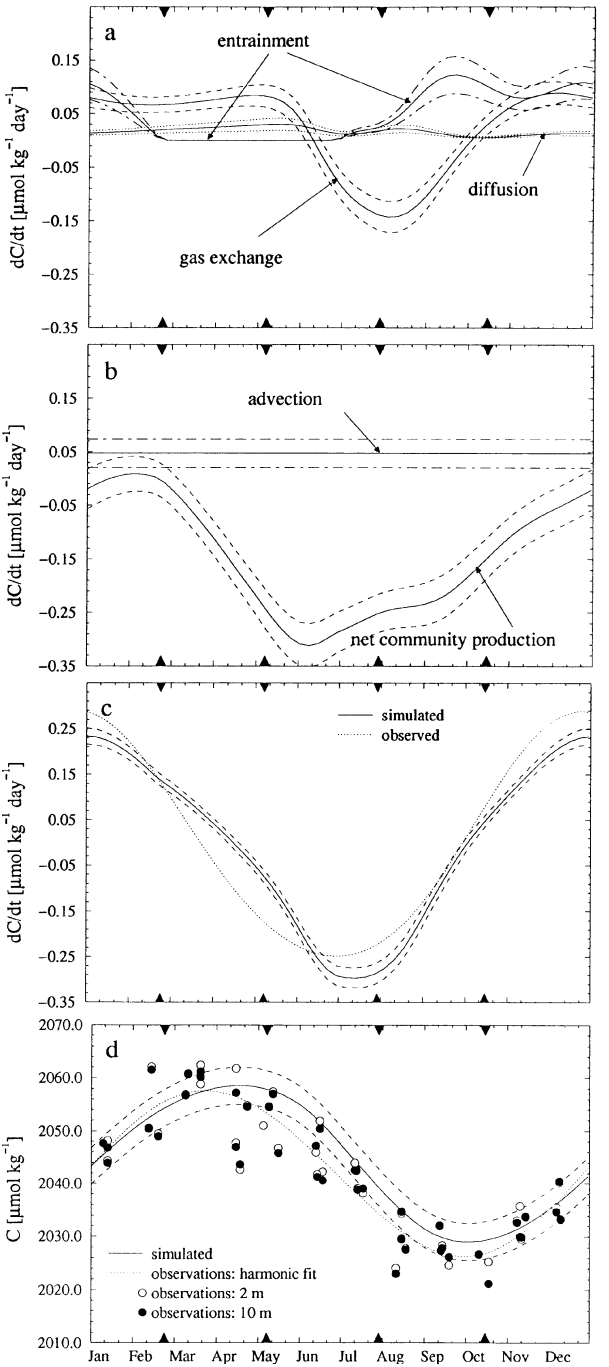
a
entrainment
diffusion
gas exchange
dC/dt [µmol kg⁻¹ day⁻¹]
0.15
0.05
−0.05
−0.15
−0.25
−0.35
b
advection
net community production
dC/dt [µmol kg⁻¹ day⁻¹]
c
simulated
observed
dC/dt [µmol kg⁻¹ day⁻¹]
0.25
d
C [µmol kg⁻¹]
2070.0
2060.0
2050.0
2040.0
2030.0
2020.0
2010.0
simulated
observations: harmonic fit
observations: 2 m
observations: 10 m
Jan Feb Mar Apr May Jun Jul Aug Sep Oct Nov Dec

Monte Carlo analysis is rather small (approximately 0.03 $\mu mol\,kg^{-1}\,d^{-1}$), compared with the errors of the individual components. This is mostly due to the compensating effect of net community production on changes in the physical processes. This behaviour exists because the $\delta^{13}C$ values of air–sea gas exchange, vertical diffusion, entrainment and advection (calculated from the ratio of ${}^{13}J_i$ and J_i) are all negative between $-8‰$ (air–sea gas exchange, diffusion and entrainment) and $-20‰$ (advection), not drastically different from the isotopic signature of net community production (about $-22‰$). Thus, any change in the magnitude of the physical processes results in a partially compensating change in net community production, which is required in order to satisfy the ${}^{13}C$ balance (4). During the period from the beginning of October to the middle of February the simulated curve is up to 0.06 $\mu mol\,kg^{-1}\,d^{-1}$ lower than the observed curve. This indicates that the contribution of one or more of the processes in the model is too small. The most likely processes causing this discrepancy are vertical entrainment and horizontal advection, because they contribute the largest part of the computed variability during this period and because their parameters are not very tightly constrained by observations. From the beginning of March until June the computed source term is up to 0.10 $\mu mol\,kg^{-1}\,d^{-1}$ higher than the observed one. Since the contribution of net community production is by far the largest during this period, it is likely that we have underestimated net community production during this period. This would be consistent with the observation that the maximum in net community production is simulated to occur one to two months later than the spring bloom.

The simulated seasonal cycle of C agrees well with the C observations and their harmonic representation (Fig. 8d). It has nearly the same amplitude as the observed, but lags in phase and fails to close exactly over the annual cycle as it should. The final value for day 366 is 3.1 $\mu mol\,kg^{-1}$ lower than the initial value for day 1. The uncertainty of the simulated curve shown in Fig. 8d has a constant value of 3.2 $\mu mol\,kg^{-1}$ and is the accumulated uncertainty calculated for the final day (day 366) of the simulation. The disagreement between the model and the observations is mostly within the uncertainties introduced by the model input variables and parameters.

Fig. 8. Results of the seasonal box model. The solid lines denote the computed curve for the standard set of parameters, and the broken lines denote the upper and lower limit of the uncertainty interval as evaluated from Monte Carlo simulations described in the text (except for (d)). The solid triangles denote the four seasons as defined in Tables 4 and 5. (a) Computed seasonal variations of the source terms of C due to air–sea gas exchange, vertical diffusion and vertical entrainment. (b) Computed seasonal variations of the source terms of C due to advection and net community production. (c) Computed seasonal variation of the rate of change of C in the mixed layer compared with the rate of change inferred from the harmonic representation of the C observations. The simulated rate of change represents the sum of the five curves shown in (a) and (b). The dotted lines represent the uncertainty range of the simulated curve. (d) Simulated and observed seasonal variations of C in the mixed layer. The circles and the dot-dashed line denote the observations, whereas the solid line represents the result of the standard simulation. The dotted lines bracket the uncertainty interval of the simulation, as given by the accumulated uncertainty on the last day of the simulation.

4.2. Mixed layer inorganic carbon budget

Tables 4 and 5 contain the integrated source terms $\mathcal{J}$ and fluxes $\mathcal{F}$ as computed by the standard version of the diagnostic model and the associated standard deviations evaluated from the Monte Carlo analysis. The source terms and fluxes have been separately integrated over 4 periods of the year, as well as over the entire annual cycle. These periods have been chosen to represent typical periods in the seasonal variability observed at BATS and are defined in Tables 4 and 5.

Over the annual period, the integrated source of net community production amounts to $-54.6 \pm 12.5\ \mu mol\,kg^{-1}$. This removal is largely compensated by inputs of entrainment $17.7 \pm 4.9\ \mu mol\,kg^{-1}$, advection $17.3 \pm 9.8\ \mu mol\,kg^{-1}$ and vertical diffusion $6.4 \pm 2.1\ \mu mol\,kg^{-1}$. Together with the annual gain of $10.1 \pm 5.9\ \mu mol\,kg^{-1}$ by air–sea gas exchange, this sums to an annual underprediction of the model of $-3.1 \pm 3.2\ \mu mol\,kg^{-1}$ (this corresponds directly to the lack of closure in Fig. 8c).

The processes air–sea exchange, vertical diffusion and entrainment are defined as fluxes at the upper and lower surface of the mixed layer box. We turn therefore to Table 5 where the temporally integrated fluxes $\mathcal{F}_i$ are listed. Air–sea gas exchange adds $1.88 \pm 0.29\ mol\,m^{-2}$ to the mixed layer during winter and spring. It removes $0.11 \pm 0.06\ mol\,m^{-2}$ in summer and fall, hence resulting in a net annual CO_2 uptake by the ocean of $1.77 \pm 0.45\ mol\,m^{-2}$. Vertical diffusion adds $0.51 \pm 0.16\ mol\,m^{-2}$ annually to the mixed layer. Over the course of one year, vertical entrainment adds $1.26 \pm 0.35\ mol\,m^{-2}$, advection adds $1.33 \pm 0.75\ mol\,m^{-2}$, and net community production removes $-2.29 \pm 0.93\ mol\,m^{-2}$. This results in an annually integrated F_{sim} of $2.58 \pm 0.27\ mol\,m^{-2}$, which is slightly less than the annually integrated F_{obs} of

Table 4
Integrated source terms, $\mathcal{J}$, as calculated by the diagnostic model for the standard run together with uncertainties estimated from the Monte Carlo analysis

Process	Spring[a] (μ mol kg^{-1})	Summer[b] (μmol kg^{-1})	Fall[c] (μmol kg^{-1})	Winter[d] (μmol kg^{-1})	Annual (μmol kg^{-1})
			Inferred from model		
$\mathcal{J}_{ex}$	6.2 ± 1.3	-1.6 ± 1.8	-4.8 ± 1.6	10.4 ± 2.4	10.1 ± 5.9
$\mathcal{J}_{diff}$	1.9 ± 0.6	1.7 ± 0.6	1.1 ± 0.3	1.7 ± 0.5	6.4 ± 2.1
$\mathcal{J}_{ent}$	0.0 ± 0.0	0.5 ± 0.2	7.1 ± 2.0	10.2 ± 2.8	17.7 ± 4.9
$\mathcal{J}_{adv}$	3.6 ± 2.0	3.9 ± 2.2	3.7 ± 2.1	6.1 ± 3.5	17.3 ± 9.8
$\mathcal{J}_{ncp}$	-8.7 ± 2.4	-23.6 ± 3.1	-16.8 ± 3.0	-5.5 ± 4.6	-54.6 ± 12.5
			Total inferred from model		
$\mathcal{J}_{sim}$	3.0 ± 0.9	-19.1 ± 1.4	-9.7 ± 1.3	22.9 ± 1.8	-3.1 ± 3.2
			Total inferred from C_{obs}		
$\mathcal{J}_{obs}$	-2.5	-19.1	-7.0	28.9	0.0

[a] Calendar day 53 to 128.
[b] Calendar day 129 to 211.
[c] Calendar day 212 to 289.
[d] Calendar day 290 to 52.

Table 5
Integrated fluxes $\mathscr{F}$ as calculated by the diagnostic model for the standard run together with uncertainties estimated from the Monte Carlo analysis

Process	Spring[a] (mol m^{-2})	Summer[b] (mol m^{-2})	Fall[c] (mol m^{-2})	Winter[d] (mol m^{-2})	Annual (mol m^{-2})
			Inferred from model		
$\mathscr{F}_{ex}$	0.75 ± 0.15	-0.00 ± 0.04	-0.11 ± 0.05	1.13 ± 0.25	1.77 ± 0.45
$\mathscr{F}_{diff}$	0.23 ± 0.08	0.04 ± 0.02	0.03 ± 0.01	0.21 ± 0.06	0.51 ± 0.16
$\mathscr{F}_{ent}$	0.00 ± 0.00	0.01 ± 0.00	0.24 ± 0.07	1.02 ± 0.28	1.26 ± 0.35
$\mathscr{F}_{adv}$	0.45 ± 0.26	0.09 ± 0.05	0.12 ± 0.07	0.68 ± 0.38	1.33 ± 0.76
$\mathscr{F}_{ncp}$	-0.86 ± 0.30	-0.54 ± 0.07	-0.51 ± 0.09	-0.37 ± 0.49	-2.29 ± 0.93
			Total inferred from model		
$\mathscr{F}_{sim}$	0.57 ± 0.11	-0.40 ± 0.03	-0.22 ± 0.04	2.66 ± 0.20	2.58 ± 0.27
			Inferred from the seasonal cycle of h and C_{obs}		
$\mathscr{F}_{obs}$	-0.03	-0.43	-0.15	3.24	2.60
$\int C(\mathrm{d}h/\mathrm{d}t)\,\mathrm{d}t$	-264.75	-62.44	66.88	260.84	-2.60
$\mathscr{F}_{tot}$	-264.78	-62.87	66.72	264.08	0.00

[a] Calendar day 53 to 128.
[b] Calendar day 129 to 211.
[c] Calendar day 212 to 289.
[d] Calendar day 290 to 52.

2.60 mol m^{-2}. The latter is caused by the covariance of the mixed layer depth and C (see above) and is balanced by the annually integrated term $C\ \mathrm{d}h/\mathrm{d}t$ (see Eq. (14)) so that the total observed annual carbon mass budget in the mixed layer, $\mathscr{F}_{tot}$, is closed.

These results depend on our decision to reduce our computed fCO_2^{oc} by 13 μatm. Restoring computed fCO_2^{oc} to their original values results over the annual period in a considerably smaller annual uptake of 1.00 ± 0.70 mol m^{-2} (-44%) and a reduced net community production of -1.90 ± 0.89 mol m^{-2} (-17%). This results in a slightly worse agreement between simulated and observed annually integrated fluxes.

4.3. The summer/fall drawdown: physical versus biological processes

The possible causes for the observed regular seasonal drawdown of C of about 30 μmol kg^{-1} from April to October observed in the mixed layer in the Sargasso Sea near Bermuda have been addressed in several recent studies. This drawdown has been attributed mainly either to biological processes (Keeling, 1993; Marchal *et al.*, 1996; Bates *et al.*, 1996b; Gruber and Keeling, 1998) or to the physical processes of advection and air–sea gas exchange (Toggweiler, 1994b). Fig. 9 displays the inorganic carbon budget of our diagnostic box model for the period from 9 May to 16 October. According to our standard model results, the observed loss of 26.1 μmol kg^{-1} in the mixed layer is predominantly due to net community production, which removes 40.4 ± 4.3 μmol kg^{-1} over this period (-36.4 ± 4.1 μmol kg^{-1} if the fCO_2^{oc} correction is removed). This estimate is comparable to the estimated net community production

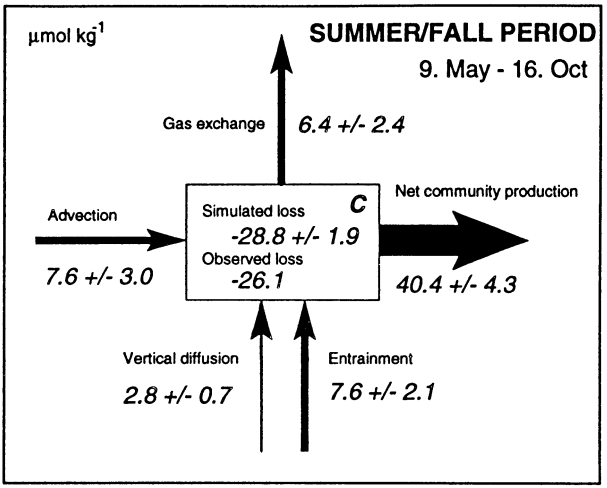

Fig. 9. Budget of dissolved inorganic carbon (C) in the mixed layer at the BATS site for the summer/fall period (9 May to 16 October). The results are given for the standard simulation of the diagnostic model together with the uncertainties as evaluated from the Monte Carlo analysis. The model infers that the observed loss of $-26.1\ \mu\mathrm{mol\,kg^{-1}}$ is mainly caused by net community production, which removes $40.4 \pm 4.3\ \mu\mathrm{mol\,kg^{-1}}$ over this period.

of Marchal *et al.* (1996), who found a value of about $-24 \pm 6\ \mu\mathrm{mol\,kg^{-1}}$ over this period. Our model therefore supports the conclusion that biological processes determine to a large part the observed summer/fall drawdown of C in the mixed layer near Bermuda (Keeling, 1993; Marchal *et al.*, 1996; Bates *et al.*, 1996b).

How firm is this conclusion? The most weakly constrained parameters in our diagnostic model are the entrainment length, l_{ent}, and the horizontal advective velocity, u. The relative uncertainty of entrainment, however, is smaller than that of advection during the summer/fall period. We therefore investigate errors associated with the horizontal velocity u only. As an extreme case, we ask how large u needs to be to explain the observed drawdown at BATS between April and October entirely by physical processes. For that purpose we ran the model in an inverse mode, by setting the simulated rate of change, $\mathrm{d}C/\mathrm{d}t$, in Eq. (2) equal to the observed rate, $\mathrm{d}C/\mathrm{d}t|_{\mathrm{obs}}$, and by solving the equation for the horizontal velocity u under the condition of zero J_{ncp}.

The required horizontal velocity u_{inv} to explain the drawdown is found to vary between about 0.33 and $-0.10\ \mathrm{m\,s^{-1}}$ (mean of $0.18\ \mathrm{m\,s^{-1}}$ between 9 May and 16 October) and is directed towards the north (see Fig. 10). This confirms the results of Bates *et al.* (1996) and Bates *et al.* (1996b), which are based on a simple mass balance. Although velocities up to $0.5\ \mathrm{m\,s^{-1}}$ have been observed at BATS (Michaels and Knap, 1996; Siegel and Deuser, 1997), they are associated with meso-scale eddies and therefore occur only over periods of a few days. The mean flow has been estimated to be from the northeast with net flow rates of less than $0.05\ \mathrm{m\,s^{-1}}$ (Olbers *et al.*, 1985; Siegel and Deuser, 1997). The inversely calculated horizontal velocities u_{inv} are

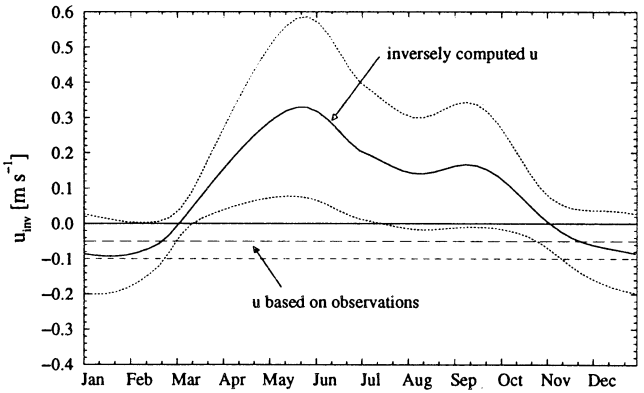

Fig. 10. Seasonal variations of the inversely computed horizontal velocity, u_{inv}, which is required in order to explain the observed seasonal variability of C in the mixed layer by physical processes alone. Also shown is the estimated mean horizontal velocity at the BATS site (Michaels and Knap, 1996; Siegel and Deuser, 1997; Olbers *et al.*, 1985) (-0.05 ± 0.05 m s^{-1}). The dotted lines denote the uncertainty interval computed for u_{inv} using the Monte Carlo analysis. The large difference between the inversely computed horizontal velocities and the observations makes it highly unlikely that the observed variability is due to physical processes alone.

therefore well above the direct estimates and are in the opposite direction. This makes it very unlikely that physical processes alone can explain the observations.

This conclusion raises difficult questions about the underlying carbon and nutrient dynamics in the mixed layer in the northwestern Sargasso Sea. Since nitrate and phosphate concentrations are near or below the analytical detection level (<0.05 μmol kg^{-1}) during the summer/fall period (Michaels *et al.*, 1994a, b; Michaels and Knap, 1996), our estimated net community production requires mechanisms that supply exogenous nutrients to the mixed layer or it requires the formation of organic matter that does not follow the classical stoichiometry (Redfield *et al.*, 1963). Assuming in the first case that carbon, nitrogen and phosphorus are taken up in the stoichiometric ratios of Anderson (1995) (C : N : P = 106 : 16 : 1), our estimated net community production during summer/fall would require 6.1 ± 0.6 μmol kg^{-1} or 0.16 ± 0.02 mol m^{-2} nitrogen and 0.38 ± 0.04 μmol kg^{-1} or 0.010 ± 0.001 mol m^{-2} phosphorus. As discussed by Marchal *et al.* (1996) and Bates *et al.* (1996b), two possible sources of exogenous nutrients are not likely to meet these nutrient requirements. One source is the supply of exogenous nutrients to the mixed layer through vertical mixing processes (diffusion and entrainment). Vertical mixing in the Sargasso Sea is quite certainly insufficient (Marchal *et al.*, 1996), since the nutricline lies below 80 m during the summer/fall period, considerably deeper than the base of the mixed layer (<50 m). The second source, atmospheric deposition of nitrogen and phosphorus to the surface ocean, may contribute significantly over short episodes (Owens *et al.*, 1992) but is much too low for a sufficient contribution to net community production over the entire period (Michaels *et al.*, 1993). It has been suggested that nitrogen fixation by diazotrophs could be responsible for at least explaining the

apparent inconsistency in the nitrogen budget (Michaels *et al.*, 1994a, b; Marchal *et al.*, 1996; Bates et al., 1996b), but available observations of the abundance of diazotrophs (*Trichodesmium spp.*) and in situ measurements of nitrogen fixation rates do not support this (Carpenter and Price, 1977; McCarthy and Carpenter, 1983; Duce, 1986; Carpenter *et al.*, 1987).

However, two recent studies based on the nutrient distribution in the thermocline of the subtropical Atlantic (Gruber and Sarmiento, 1997) and BATS (Michaels *et al.*, 1996) show that nitrogen fixation in the subtropical North Atlantic may be much higher than indicated above and may introduce annually $0.072\,\mathrm{mol\,N\,m^{-2}}$ or $0.133–0.230\,\mathrm{mol\,N\,m^{-2}}$ of exogenous nitrogen into the mixed layer. This is sufficient to meet most or all of the biological nitrogen requirement at BATS estimated in the present study, provided that this input occurs over the course of the summer/fall period. It remains unclear, however, how these diazotrophs obtain the required phosphate. Karl *et al.* (1992) proposed that *Trichodesmium spp.* may be able to transfer phosphorus between the nutricline and the ocean's surface by active regulation of its buoyancy. The cycle starts at depth, where *Trichodesmium spp.* takes up phosphorus in excess of its demand, then ascends to the surface, where it fixes nitrogen until it becomes negatively buoyant because of the exhaustion of phosphorus and accumulation of carbohydrates. However, the significance of this transport mechanism and the possible contribution of the vertical migration of other organisms is not established yet.

Alternatively, the uptake and release of carbon, nitrogen and phosphorus by the plankton community may occur at non-traditional elemental stoichiometries (Sambrotto *et al.*, 1993; Toggweiler, 1993; Lueker *et al.*, 1997). Such uncoupling between carbon and nitrogen uptake and release was also found by Banse (1994), who, reevaluated two closed-system experiments conducted in the 1960s (McAllister *et al.*, 1961; Antia *et al.*, (1963). Production of relatively nitrogen poor organic matter thus may be capable of supporting net CO_2 uptake under extremely low nutrient concentrations. The precision of the determination of the carbon to nitrogen ratios in organic matter (especially dissolved) at BATS have not yet reached a level to rule out this possibility (Michaels and Knap, 1996).

Our diagnostic model does not furnish a clear answer to most of these questions, but it does show, clearly that net community production is the controlling process in generating the observed drawdown of C in the mixed layer between May and October in the northwestern Sargasso Sea.

4.4. Comparison with other studies

The annual net uptake of atmospheric CO_2 at BATS indicated by our model calculations is $1.77 \pm 0.45\,\mathrm{mol\,m^{-2}}$ (see Table 5). If the fCO_2^{nc} correction were removed, a substantially smaller annual uptake of $1.00 \pm 0.38\,\mathrm{mol\,m^{-2}}$ would be obtained.

Bates *et al.* (1996b) estimated the annual air–sea gas exchange flux individually for the years 1991–1993 using both a formulation of Tans *et al.* (1990) and Liss and Merlivat (1986) for the calculation of the gas exchange velocity, k. They found a

considerably smaller average annual ocean uptake of 0.22–0.83 mol m^{-2}. The difference between the two estimates is mainly due to the lowering of our calculated fCO_2^{oc}. Additional differences are caused by the use of two different wind speed data sets. Bates *et al.* (1996b) used daily average wind speed data from the U.S. Naval Air Station on Bermuda, whereas our estimate is based on climatological wind speed data from Isemer and Hasse (1985), which are on average about 1–2 m s^{-1} higher. Marchal (1996) calculated a net uptake of CO_2 between February and December 1989 of approximately 0.25 mol m^{-2}. This is again considerably lower than our estimate for this 10 month period (1.00 $\pm$ 0.32) mol m^{-2}. The difference here is also mainly due to our lowered fCO_2^{oc} and the use of different wind data. Marchal (1996) used a record measured at St. Davids Head on the east end of Bermuda, which are also up to 3 m s^{-1} smaller than the climatological winds.

Without having direct fCO_2^{oc} and wind-speed measurements available for the BATS site, it is difficult to resolve which calculated fCO_2^{oc} and wind-speed data sets are the most appropriate to use. Doney (1996) recently suggested that winds from the European Centre for Medium Range Weather Forecasts (ECMWF) operational analysis provide a good basis for estimating wind speeds at the BATS site. These analyzed winds agree well with wind speed records from Bermuda airport but are on average 1 to 2 m s^{-1} lower than those of Isemer and Hasse (1985) (Doney, 1996).

We found in our study at the nearby station 'S' for the years 1983–1989 a very similar annual uptake of 1.79 mol m^{-2} (Gruber and Keeling, 1998). This agreement is as expected, since both applied a similar correction to their calculated fCO_2^{oc} and both used the same climatological wind speeds. In summary, all studies predict within the uncertainties that the area in the vicinity of Bermuda is a weak to moderate oceanic sink for atmospheric CO_2.

The air–sea exchange flux at BATS is composed of a natural flux and an anthropogenic perturbation flux. The latter is estimated at about 0.47 mol m^{-2} for the period 1991–1994 on the basis of the three-dimensional Princeton ocean biogeochemistry model (Sarmiento *et al.*, 1995) (26°N–36°N and 69°W–59°W). Nearly the same value is obtained by distributing the model estimated anthropogenic CO_2 uptake for this period (2.3 Pg C yr^{-1}) evenly over the entire surface area of the ocean (0.5 mol m^{-2}). The remaining annual natural flux into the ocean of about 1.30 $\pm$ 0.45 mol m^{-2} is probably associated with the subduction of waters in this recirculation region of the subtropical gyre of the North Atlantic (Follows *et al.*, 1996; Follows, 1996). According to this hypothesis strong meridional gradients in mixed layer depth at the end of winter enhance the subduction of cold, carbon-rich waters into the main thermocline and hence increased air-to-sea fluxes of CO_2. This is a different mechanism than that of Winn *et al.* (1994), who argued that Ekman transport towards the subtropical convergence is the main mechanism for explaining the net CO_2 uptake at the HOT station north of Hawaii, although these authors did not attempt to separate the anthropogenic from the natural component.

It is instructive to compare our annual estimate of net community production in the mixed layer of 2.3 $\pm$ 0.9 mol m^{-2} (1.9 $\pm$ 0.9 mol m^{-2} when fCO_2^{oc} is restored) with other studies that addressed new production and net community production in the waters near Bermuda. A summary of these estimates is given in Table 6. It is

Table 6
Summary of estimates of annual biological production in the Sargasso Sea at 'S' and BATS stations

Author	Type of production[a]	Estimate, (mol C m^{-2})	Location	Method
Platt and Harrison (1985)	NP in euphotic layer	2.8–3.7[b]	'S'	Nitrate based f-ratio
Jenkins and Goldman (1985)	NP in euphotic layer	2.9–4.2[c]	'S'	Seasonal oxygen cycle
Musgrave *et al.* (1988)	NP in euphotic layer	2.1–2.8[c]	'S'	Seasonal oxygen cycle
Spritzer and Jenkins (1989)	NP in euphotic layer	3.1–4.0[c]	'S'	O_2, Ar and He cycles
Altabet (1989)	Downward flux of PN	2.5[d]	BATS	Sediment traps and PN cycle
Lohrenz *et al.* (1992)	Downward flux of POC	1.2	BATS	Sediment traps
Carlson *et al.* (1994)	Downward flux of DOC	1.1	BATS	DOC cycle
Fasham *et al.* (1990)	NP in mixed layer	2.9[e]	'S'	Mixed layer ecosystem model
Marchal *et al.* (1996)	NCP in mixed layer	1.2 ± 0.3[f]	BATS	Diagn. mixed layer model
Gruber and Keeling (1998)	NCP in mixed layer	0.9 ± 0.4	'S'	Diagn. mixed layer model
This study (1998)	NCP in mixed layer	2.3 ± 0.9	BATS	Diagn. mixed layer model
	NCP in euphotic layer	3.8[g]	BATS	Extrapolation

[a] NP, New Production; NCP, Net Community Production; PN, Particulate Nitrogen; POC, Particulate Organic Carbon; DOC, Dissolved Organic Carbon.
[b] Based on weighted average *f*-ratio of 0.31 and primary production estimate of Lohrenz *et al.* (1992).
[c] Conversion of oxygen to carbon based on $-O_2$:C ratio of Anderson and Sarmiento (1994).
[d] Combined estimate of downward flux of sinking PN and suspended PN, converted from nitrogen to carbon using the N:C ratio of Anderson and Sarmiento (1994).
[e] Conversion of nitrogen to carbon based on N:C ratio of Anderson and Sarmiento (1994).
[f] Extrapolation of the estimated mean net community production between April and October (186 days) to the entire year.
[g] Tentative extrapolation of our mixed layer estimate assuming that 40% of the annual net community production occurs below the mixed layer (Marchal *et al.*, 1996).

important to note that the concepts of net community production and new production are, however, not strictly equivalent (Williams, 1993), unless we assume a steady state over the annual cycle (Martin *et al.*, 1987; Platt *et al.*, 1989; Laws, 1991).

The only estimates of biological production that pertain to the mixed layer are those of Marchal *et al.* (1996), Fasham *et al.* (1990) and our previous study at Station 'S' (Gruber and Keeling, 1998). Marchal *et al.* (1996) estimated the net community production with a diagnostic carbon model coupled to a one-dimensional turbulent closure model. They found for the period from April to October 1989 (186 days) a value of about $0.60 \pm 0.15\,\mathrm{mol\,m^{-2}}$. This is significantly lower than our estimate of $1.05 \pm 0.11\,\mathrm{mol\,m^{-2}}$ over the period from May to October (161 days). Based on a nitrogen cycle model of the plankton dynamics in the mixed layer at station 'S', Fasham *et al.* (1990) estimated the annual new production in the mixed layer to be about $2.9\,\mathrm{mol\,C\,m^{-2}}$ (converted to carbon using a C:N ratio of 117:16). This is significantly higher than our annual estimate of net community production. A possible cause for at least part of the discrepancy may be due to their overestimating of the nitrate transport into the mixed layer by assuming a constant nitrate concentration below the mixed layer (see also discussion by Hurtt and Armstrong (1996)). Gruber and Keeling (1998) inferred in their diagnostic study of the carbon cycle at station 'S' for the years 1983–1989 an annual net community production in the mixed layer of $0.9 \pm 0.5\,\mathrm{mol\,m^{-2}}$. This is less than half of our value found for BATS, but not inconsistent given the large uncertainty ranges. The difference between these two diagnostic studies stems almost entirely from the inclusion of advection in the present study.

To obtain a first estimate of net community production over the entire euphotic layer, we tentatively extrapolate our mixed layer estimate to the whole euphotic layer by accepting an estimate of Marchal *et al.* (1996), that about 40% of the annual net community production occurs below the mixed layer. This extrapolation is done only for comparing our estimate with previous studies since the above fraction is highly uncertain. We obtain an annual euphotic net community production on the order of $3.8\,\mathrm{mol\,m^{-2}}$. This estimate is substantially higher than estimates of export production based on the combined downward flux of particulate organic carbon (POC) and dissolved organic carbon (DOC) ($2.3\,\mathrm{mol\,m^{-2}}$) (Lohrenz *et al.*, 1992; Carlson *et al.*, 1994) and based on the total downward flux of particulate nitrogen ($2.5\,\mathrm{mol\,m^{-2}}$) (Altabet, 1989). Our estimated euphotic net community production is comparable to the estimates of new production of about 3–4 $\mathrm{mol\,m^{-2}}$ based either on in situ changes of oxygen alone (Jenkins and Goldman, 1985; Musgrave *et al.*, 1988) or in combination with concomitant argon and helium data (Spitzer and Jenkins, 1989). Good agreement is also found if we apply the estimated f-ratio of Platt and Harrison (1985) (0.31) to the modern ^{14}C based annual primary production estimate (9–12 $\mathrm{mol\,m^{-2}}$) (Lohrenz *et al.*, 1992) to get an annual new production estimate of 2.8–3.7 $\mathrm{mol\,m^{-2}}$. Thus, our diagnostically inferred annual net community production at the BATS site is within the broad range of previous estimates of new and net community production based on a wide range of methods.

5. Summary and conclusions

The observed mean seasonal cycle of dissolved inorganic carbon (C) in the mixed layer at the U.S. JGOFS Bermuda Atlantic Time-series Study (BATS) site between 1991 and 1994 is the result of a complex interplay of biological processes (net community production) and physical processes (air–sea gas exchange, vertical diffusion, entrainment and horizontal advection). We assessed the relative contributions of these processes quantitatively using a diagnostic box model of the mixed layer inorganic carbon system and constraints from concurrent observations of $\delta^{13}C$.

During the summer/fall period from 9 May to 16 October, the C concentration in the mixed layer decreases by about 26 $\mu mol\,kg^{-1}$. This occurs in the absence of measurable nitrate and phosphate. We attribute the decrease in C mostly to net community production (-40 ± 4) $\mu mol\,kg^{-1}$. This requires mechanisms that either supply exogenous nutrients to the mixed layer or allow that net community production occurs with very little addition of nutrients. Vertical transport of nutrients from the nutricline by physical processes and deposition at the sea-surface from the atmosphere appear to be insufficient to meet the nutrient demand. The importance of nitrogen fixation for the nitrogen budget in the euphotic layer near Bermuda was historically considered to be too small. Two recent studies based on the nutrient distribution in the thermocline suggest, however, that N_2 fixation in the subtropical North Atlantic may be much larger and supply sufficient nitrogen to the mixed layer to explain the observed drawdown. *Trichodesmium spp.*, the most important pelagic diazotroph, can actively regulate its buoyancy, which may permit a transport of the required phosphate between the nutricline and the surface mixed layer, but the importance of this mechanism is not known.

Our estimate of the annual net community production in the mixed layer at BATS (55 ± 13 $\mu mol\,kg^{-1}$ or 2.3 ± 0.9 $mol\,m^{-2}$) is comparable with previous estimates of net community production and new production in this layer. A tentative extrapolation of our annual mixed layer estimate to the entire euphotic layer yields an annual estimate on the order of 3.8 $mol\,m^{-2}$. This is well within the range of previous new production estimates obtained by a wide variety of methods. Adequate measurements of the seasonal cycle of C and $\delta^{13}C$ over the entire water column would permit extension of our diagnostic model over the entire upper ocean and allow an estimate of the net community production in the entire euphotic layer with considerably smaller errors.

We compute a moderate sink for atmospheric CO_2 (1.8 ± 0.5 $mol\,m^{-2}$) at BATS, consistent with previous estimates for this station. Results from the 3-D Princeton ocean biogeochemistry model show that about 25% of this flux is due to the uptake of anthropogenic CO_2 from the atmosphere, while the remainder is probably associated with the subduction of waters in this recirculation region of the subtropical gyre.

The time-series measurements of the inorganic carbon system in the mixed layer near Bermuda offer the possibility to look not only at the average seasonal cycle but also at longer term variability (e.g. Bacastow *et al.* (1996)). Our analysis of the average seasonal cycle for the years 1991 to 1994 may help in the interpretation of such records, including the uptake of anthropogenic CO_2 by the oceans and climatic

variability. In 1983, one of us (CDK) started to take monthly to bimonthly samples at the nearby station 'S', providing now the longest time-series of C in the world oceans. The overlap of the new time-series from BATS with station 'S' series now covers five years, allowing us in the future to investigate differences between these two stations and eventually to link the two.

Acknowledgements

We are greatful to A.H. Knap, A.F. Michaels, N.R. Bates and other staff of the Bermuda Biological Station for Research for their continuing assistance in providing water samples, in logistics and in data interpretation. We also wish to express our gratitude to T. Lueker, G. Emanuele, A. Bollenbacher, K. Egan and B. Stewart of the Carbon Dioxide Research Group at the Scripps Institution of Oceanography, who performed the carbon system analysis and data management. We are deeply indebted to O. Marchal for many inspiring and helpful discussions during the preparation of this article. A detailed review by N.R. Bates and remarks from three anonymous reviewers helped to improve the manuscript. We thank J.L. Sarmiento, who provided the code of the 3-D Princeton ocean biogeochemistry model, and the Centro Svizzero di Calcolo Scientifio (CSCS) for providing computer time. N.G. and T.F.S. were supported by the Swiss National Science Foundation. The measurements and their preparation in a database were made possible via the grant ATM-91-21938 of the U.S. National Science Foundation.

Appendix A. Sampling and methods

Personnel from the Bermuda Biological Station for Research (BBSR) sampled the sea water at the BATS station for us in duplicate at approximately 2 and 10 m depth. The bottles were then shipped to the laboratory at the Scripps Institution of Oceanography, where they were stored in the dark until analysis. Measurement procedures for dissolved inorganic carbon (C), total titration alkalinity (Alk) and the $^{13}C/^{12}C$ ratio of C are described in detail by Lueker *et al.* (1997). Briefly, C was measured using a cryogenic vacuum extraction followed by a manometric determination of the extracted pure CO_2 gas. The imprecision of the C determination is about ± 0.6 μmol kg^{-1}. The inaccuracy has been estimated to be about ± 1 μmol kg^{-1} (Lueker *et al.*, 1997). Alk was determined using a closed cell potentiometric titration with an estimated imprecision of ± 1 μmol kg^{-1} and an inaccuracy of less than ± 5 μmol kg^{-1}. The $^{13}C/^{12}C$ ratio of C was only measured on samples collected at approximately 10 m depth. This ratio is determined on the same extracted pure CO_2 gas as used for the manometric measurement of C. The samples were run on a VG prism isotope mass spectrometer at the Isotope Laboratory of the Scripps Institution of Oceanography. We report the $^{13}C/^{12}C$ isotopic ratio of C by the reduced ratio, $\delta^{13}C$, defined as

$$\delta^{13}C = \frac{{}^{13}r - {}^{13}r_s}{{}^{13}r_s}, \tag{A.1}$$

Table 7
Summary of inorganic carbon system observations at the U.S. JGOFS Time-series station BATS from 1990 to 1994

Sta	Date	z (m)	T (°C)	S	C (μmol kg^{-1})	Δ	Flag[a]	Alk (μmol kg^{-1})	Δ	Flag[a]	$\delta^{13}C$ (‰)	Δ	Flag[a]	$fCO_2^{oc\,b}$ (μatm)
21	900622	1	24.99	36.455	2031.94	1.96		2384.17	1.21					349
21	900622	10	24.33	36.465	2031.79	0.95		2378.03	4.36		1.40	0.02		347
22	900718	2	27.35	36.452	2030.62	0.58		2378.91	0.15					386
22	900718	10	27.25	36.484	2030.89	0.40		2377.16	0.39		1.39	0.01		388
23	900814	1	28.11	36.604	2021.44	0.23		2392.30	0.48					364
23	900814	10	27.97	36.579	2021.33		S	2388.81	2.88		1.39	0.12	F	367
24	900911	3	29.04	36.467	2013.33	0.32		2384.23		S				374
24	900911	11	28.31	36.456	2013.68	0.27		2379.64	1.52		1.47	0.01		370
25	901015	1	25.88	36.483	2019.34	0.34		2388.98	1.22					335
25	901015	11	28.51	36.466	2019.60	1.15		2386.34	0.06		1.51	0.02		374
26	901105	2	24.66	36.655	2027.88	0.55		2396.92	2.53					325
26	901105	11	24.66	36.657	2026.92	1.21		2393.79	0.27		1.50	0.02		327
27	901204	2	22.94	36.740	2035.58		S	2403.93	0.46					308
27	901204	10	22.94	36.738	2034.22	0.55		2402.69	1.12		1.47	0.02		307
30	910321	2	19.40	36.609	2062.96	0.71		2393.98	4.37					310
30	910321	11	19.24	36.609	2063.48	2.09	F	2391.34	9.69	F	1.28	0.05		315
31	910416	1	19.78	36.641	2064.08	1.92								
31	910416	9	19.72	36.633	2061.45	0.60		2390.25	3.05		1.27		S	319
32	910513	2	20.50	36.624	2060.41	2.46	F	2391.60	0.94					325
32	910513	11	20.38	36.618	2059.89		S	2392.62	6.08	F	1.34	0.03		322
33	910619	4	25.34	36.681	2046.80	0.06				S				
33	910619	10	24.96	36.679	2046.49	0.55		2396.25	2.65		1.37	0.01		358
34	910715	1	27.44	36.430	2032.80	0.46		2384.43		S				383
34	910715	10	27.20	36.476	2030.90	0.22		2381.64	0.20		1.41	0.00		381
35	910812	1	29.57	36.858	2040.56	0.09		2408.39	1.65					398
35	910812	9	28.97	36.921	2043.14	0.09		2414.39	0.98		1.42	0.01		388
36	910913	1	26.74	36.243	2019.83	1.01		2379.62	0.24					357
36	910913	10	26.41	36.403	2020.20	0.25		2376.17	2.84		1.45	0.01		358
38	911111	2	23.36	36.568	2033.97	0.94								

38	911111	10	23.36	36.566	2032.73	0.23		2394.39	1.43		1.45	0.02	317
39	911210	1	22.65	36.804	2044.72	0.18							
39	911210	12	22.66	36.788	2043.28	0.39		2401.38	0.85		1.43	0.00	318
40	920109	3	20.73	36.697	2053.22	0.34		2398.90	0.22				308
40	920109	21	20.72	36.695	2052.92	1.05		2397.80	3.04		1.35	0.02	309
41	920213	1	19.29	36.677	2066.47	0.36							
41	920213	9	19.30	36.681	2065.86	0.12		2398.52	0.04		1.25	0.02	309
42	920310	2	19.61	36.659	2060.18	0.18							
42	920310	10	19.62	36.673	2060.28	0.82		2395.13	1.43		1.28	0.01	309
43	920424	1	20.62	36.786	2065.27	0.05							
43	920424	11	20.49	36.767	2064.51	0.27		2401.74	0.50		1.28	0.00	319
43	920506	3	21.12	36.788	2062.06	0.89		2405.38	0.17				321
45	920617	2	23.51	36.392	2040.25	1.44							
45	920617	11	23.51	36.405	2039.78	0.05		2379.35	4.32	F	1.34	0.02	347
46	920714	1	26.38	36.382	2030.49	0.19							
46	920714	9	26.35	36.382	2030.68	0.20		2378.27	2.81		1.36	0.00	372
47	920816	2	28.48	36.408	2019.27	1.44		2378.08	3.71				382
47	920816	9	28.04	36.424	2020.27	0.29		2379.54	0.40		1.39	0.01	376
48	920915	1	27.12	36.299	2011.70	0.18							
48	920915	11	26.78	36.283	2011.22	0.57		2375.84	2.72		1.48	0.02	349
50	921112	2	23.72	36.564	2027.59	1.11							
50	921112	11	23.75	36.543	2026.60	0.00		2390.73	2.93		1.45	0.01	316
51	921209	1	21.92	36.564	2038.23	0.33							
51	921209	10	21.92	36.563	2038.39	0.55		2387.35	1.32		1.38	0.03	314
52	930112	1	21.10	36.659	2047.74	0.79		2396.02	5.31	F			308
52	930112	11	20.99	36.655	2047.18	0.33		2396.20	0.08		1.30	0.02	306
53	930211	1	20.11	36.682	2055.15	0.50		2396.33	4.36	F			306
53	930211	11	20.11	36.682	2055.04	0.62		2398.98	2.01		1.26	0.02	303
54	930312	1	19.27	36.789	2063.58	3.04	F	2393.25	0.19				311
54	930312	11	19.20	36.637	2062.66	0.48		2393.75	2.05		1.20	0.02	308
55	930416	4	20.86	36.761	2056.78	1.31							
55	930416	9	20.85	36.763	2055.77	0.45		2403.00	2.73		1.27	0.02	310
56	930510	5	20.94	36.563	2052.55	1.69							
56	930510	11	20.94	36.581	2052.59	1.44		2389.02	0.24		1.26	0.02	321
57	930615	4	23.91	36.761	2050.74	0.06							

(*continued on next page*)

Table 7 (*continued*)

Sta	Date	z (m)	T (°C)	S	C (μmol kg^{-1})	Δ	Flag[a]	Alk (μmol kg^{-1})	Δ	Flag[a]	$\delta^{13}C$ (‰)	Δ	Flag[a]	fCO_2^{oc}[b] (μatm)
57	930615	11	23.90	36.760	2050.21	0.05		2401.76	2.23		1.25	0.01		343
58	930713	1	26.77	36.749	2052.31	0.16								
58	930713	10	26.36	36.770	2052.40	1.04		2402.79	1.29		1.27	0.00		380
59	930819	2	27.53	36.668	2031.62	0.74								
59	930819	10	27.52	36.666	2031.46	0.28		2397.00	2.93		1.40		S	368
60	930914	2	27.21	36.418	2017.36	0.45								
60	930914	11	27.18	36.417	2017.23	0.72		2380.63	0.72		1.44	0.01		358
61	931012	2	26.02	36.437	2017.66	0.36								
61	931012	10	25.95	36.434	2017.60	0.57		2378.31	1.08		1.48	0.01		345
62	931109	2	24.94	36.514	2028.32		S							
62	931109	11	24.84	36.512	2027.78	0.17		2388.06	0.45		1.39	0.00		335
63	931207	2	23.29	36.463	2027.93	0.84								
63	931207	10	23.29	36.461	2026.96	0.02		2383.67	0.77		1.42	0.03		319
64	940112	2	20.90	36.558	2045.84	0.63								
64	940112	10	20.91	36.557	2044.78	0.35		2389.83	0.67		1.34	0.03		309
65	940218	1	20.35	36.614	2050.25	0.41								
65	940218	10	20.36	36.613	2049.83	1.16		2394.57	0.19		1.29	0.02		304
66	940321	2	19.40	36.576	2057.50	0.95								
66	940321	11	19.39	36.576	2058.75	0.20		2390.65	0.23		1.20	0.02		308
67	940419	2	21.78	36.783	2052.90	0.59								
67	940419	11	21.53	36.777	2053.55	0.33		2403.90	0.82		1.31	0.03		315
68	940517	1	23.31	36.593	2046.40	2.88	F							
68	940517	11	23.27	36.592	2046.13	1.17		2391.88	3.80		1.29	0.01		339
69	940614	3	25.25	36.364	2032.80	0.30								
69	940614	10	24.21	36.401	2036.08	0.25		2378.27	0.13		1.30	0.01		351
70	940719	1	28.48	36.531	2034.11	1.17		2384.40	0.01					401
70	940719	10	28.12	36.534	2035.31	0.69		2385.37	2.88		1.36	0.03		397
71	940816	1	28.59	36.552	2031.72	0.91								
71	940816	11	28.31	36.543	2031.48	1.39		2386.31	0.39		1.33	0.02		392
72	940920	1	27.23	36.366	2011.76	1.06								
72	940920	11	27.16	36.363	2013.01	0.70		2381.75	0.10		1.42	0.03		349

73	941019	3	24.25	36.540	2022.00		S						
73	941019	10	24.24	36.538	2017.60	0.23		2384.75	4.80	F	1.48	0.01	317
74	941115	1	22.91	36.659	2037.10	2.64	F						
74	941115	11	22.91	36.656	2036.60	0.16		2398.16	1.02		1.38	0.00	313
75	941209	3	22.45	36.676	2039.56	6.39	F						
75	941209	10	22.45	36.674	2038.78	4.20	F	2395.21	0.17		1.35	0.06	313

[a] Flags: S = single sample analysis result; F = flagged value because difference between single sample results exceeded 4-σ of measurement precision (Lueker et al., 1997) ($\sigma_C = 0.5\ \mu mol\ kg^{-1}$, $\sigma_{Alk} = 1\ \mu mol\ kg^{-1}$, $\sigma_{\delta^{13}C} = 0.02‰$).

[b] Computed from temperature, salinity, dissolved inorganic carbon, alkalinity and nutrients using the routines of Fink (1996). The calculated values were then reduced by 13 µatm to agree closely with direct observations (see also text).

where ^{13}r denotes the $^{13}C/^{12}C$ ratio of the sample, and $^{13}r_s$ the $^{13}C/^{12}C$ ratio of the Pee Dee belemnite standard (Craig, 1957; Mook and Grootes, 1973). The imprecision and inaccuracy of the $\delta^{13}C$ analysis were estimated to be $\pm 0.02‰$, and $\pm 0.1‰$, respectively (Lueker *et al.*, 1997).

The CO_2 fugacity in the mixed layer (fCO_2^{oc}) was calculated from the CDRG *C* and *Alk* data using the procedures developed by Fink (1996) and temperature, salinity, phosphate and silicate data from BBSR (Knap *et al.*, 1993, 1994). We used the dissociation constants of Dickson and Millero (1987) for carbonic acid, of Dickson (1990) for boric acid, of Millero (1995) for water in seawater, of Dickson and Riley (1979) for phosphoric acid, and of Millero (1995) for silicic acid. The CO_2 solubility is computed from the formula given by Weiss (1974). The total boron is estimated from a linear relationship with salinity given by Uppström (1974). The calculated fCO_2^{oc} values were reduced by 13 μatm, based on a comparison of direct measurements of fCO_2^{oc} at sea. Samples were collected on Leg 0 of the South Atlantic Ventilation Experiment (SAVE) in 1987 and analyzed identically as those reported here. Calculated, fCO_2 were then compared with direct measurements of fCO_2^{oc} carried out using a head-space equilibrator (Takahashi *et al.*, 1993) and a flow-through equilibrator (Weiss, 1981) (see Lueker *et al.* (1997) for details).

The measured and calculated carbon system parameters from 1990 to 1994 obtained at the U.S. JGOFS BATS station are tabulated numerically in Table 7.

Appendix B. Monte Carlo simulations

For the Monte Carlo simulations, we produce 2000 realizations each with a set of model parameters whose values are chosen randomly but assumed to be Gauss distributed with prescribed mean and standard deviation (Table 8). At every point in time and for every model output variable, an uncertainty interval is obtained by calculating a weighted standard deviation (67% within this interval). The weighting is introduced to take into consideration that the simulated *C* is constrained by the observations, and therefore parameter sets that produce very unrealistic seasonal patterns are weighted less than those that fit the observations closely. The weighting is done by a cost function (Q) given by:

$$Q = \frac{1}{365}\sum_{i=1}^{365}(C^{sim} - C^{obs})^2 \frac{1}{\sigma_C^2}, \tag{B.1}$$

where σ_C is the estimated total uncertainty in the determination of *C*, chosen to be 2 μmol kg^{-1}. The weighting factor w_i of each run i is

$$w_i = \exp\left(-\frac{(Q_i - Q_{std})^2}{\sigma_Q^2}\right), \tag{B2}$$

where Q_{std} is the value of the cost function for the standard run ($Q_{std} = 0.9$) and σ_Q the standard deviation of the cost function ($\sigma_Q = 3.0$). The weighting reduces the calculated uncertainties of the integrated fluxes and source terms by about 40%.

Table 8
Initial values and uncertainties of parameters used for the Monte Carlo simulations

Parameter	Standard value	Standard deviation	Unit	Description
$d\delta^{13}C/dC\|_{tc}$	-0.0052	0.0008	$‰\ \mu mol^{-1}\ kg$	Ratio of vertical $\delta^{13}C$ and C gradient
l_{ent}	12	6	m	Length scale of entrainemt
u	-0.05	0.05	$m\ s^{-1}$	Mean horizontal velocity
dC/dx	1.1×10^{-5}	0.3×10^{-5}	$\mu mol\ kg^{-1}\ m^{-1}$	Mean horizontal C gradient
$d\delta^{13}C/dx$	-1.2×10^{-7}	1.2×10^{-7}	$‰\ m^{-1}$	Mean horizontal $\delta^{13}C$ gradient
β_{ex}	1.0	0.3		Multiplication factor for gas exchange
β_{diff}	1.0	0.5		Multiplication factor for vert. diffusion
ΔfCO_2^{oc}	0	10	µatm	Correction term for fCO_2^{oc}
$\Delta dC/dz\|_{tc}$	0.0	0.1	$\mu mol\ kg^{-1}\ m^{-1}$	Correction term for $dC/dz\|_{tc}$

The model parameters $d\delta^{13}C/dC|_{tc}$, $d\delta^{13}C/dx$, l_{ent}, u and dC/dx (see Table 8) are poorly constrained by direct observations. Additional uncertainties are associated with the parameterization of air–sea gas exchange and vertical diffusion, with the calculation of fCO_2^{oc}, with the determination of the vertical C gradient, and with the estimation of the $^{13}C/^{12}C$ ratio of organic matter. To capture these uncertainties we introduce additional parameters (see Table 8). The parameters β_{ex} and β_{diff} represent multiplication factors that permit us to modify the source term of air-sea gas exchange (J_{ex} and $^{13}J_{ex}$) and vertical diffusion (J_{diff} and $^{13}J_{diff}$). We also introduce the modification parameters ΔfCO_2^{oc}, $\Delta dC/dz|_{tc}$, and $\Delta^{13}r_{org}$, which are added to fCO_2^{oc}, $dC/dz|_{tc}$ and $^{13}r_{org}$ to permit random variations of these variables. A summary of these parameters together with their standard values and uncertainties is given in Table 8. The standard values of $d\delta^{13}C/dC|_{tc}$, $d\delta^{13}C/dx$, l_{ent}, u and dC/dx are those adopted for the standard run and for which the estimated uncertainties are discussed in the parameter section above. By definition, the standard values of the β terms are 1.0, and the standard values of the modification terms ΔfCO_2^{oc}, $\Delta dC/dz|_{tc}$, and $\Delta^{13}r_{org}$ are 0.

Uncertainties in thermodynamic relationships and dissociation constants of the CO_2 system in seawater can introduce significant errors in calculating fCO_2^{oc} from other parameters (Millero *et al.*, 1993; Fink, 1996). We have tried to minimize the errors from these by calibrating our calculated fCO_2^{oc} with direct observations. However, our applied correction of 10 µatm demonstrates the level of uncertainty, and therefore a standard deviation of 10 µatm is assigned to these calculated values and hence to ΔfCO_2^{oc}. Furthermore the calculation of the gas exchange velocity from wind speed is also uncertain. An uncertainty of 30 is assumed in this respect to provide error constraints for β_{ex} (Wanninkhof, 1992; Marchal, *et al.*, 1996).

We assign an uncertainty of 0.1 $\mu mol\ kg^{-1}\ m^{-1}$ to the determination of the vertical C gradient below the mixed layer from the observations. This corresponds to the

standard deviation of the harmonic fit to the observations in Fig. 6a. We estimate that the determination of the value of the vertical diffusion coefficient, K_z, from Eq. (17) is not better than 50%. Therefore, a value of 0.5 is used for the uncertainty of β_{diff}.

We estimate the error in the determination of $^{13}r_{\text{org}}$ from the observed $\delta^{13}C$ variability of marine phytoplankton. Over the temperature range found at Bermuda (19–28°C), Rau *et al.*, (1989) reported a variation of $\delta^{13}C_{\text{org}}$ of $\pm 2‰$. We include the possibility of an over looked small fractionation of $\pm 1‰$ during respiration, thus resulting in an overall uncertainty of $\delta^{13}C_{\text{org}}$ of $\pm 3‰$. This corresponds to an uncertainty of 3×10^{-5} for $^{13}r_{\text{org}}$.

References

Altabet, M.A., 1989. Particulate new nitrogen in the Sargasso Sea, Journal of Geophysical Research 94(C9), 12771–12779.

Anderson, L.A., 1995. On the hydrogen and oxygen content of marine phytoplankton. Deep-Sea Research I 42(9), 1675–1680.

Anderson, L.A., Sarmiento, J.L., 1994. Redfield ratios of remineralization determined by nutrient data analysis. Global Biogeochemistry Cycles 8(1), 65–80.

Antia, N.J., McAllister, C.D., Parsons, T.R., Stephens, K., Strickland, J.D.H., 1963. Further measurements of primary production using a large volume plastic sphere. Limnology and Oceanography 8, 166–183.

Bacastow, B., Maier-Reimer, E., 1991. Dissolved organic carbon in modeling oceanic new production. Global Biogeochemical Cycles 5(1), 71–85.

Bacastow, R.B., Keeling, C.D., Lueker, T.J., Wahlen, M., Mook, W.G., 1996. The ^{13}C Suess effect in the world surface oceans and its implications for oceanic uptake of CO_2: Analysis of observations at Bermuda. Global Biogeochemical Cycles 10(2), 335–346.

Banse, K., 1994. Uptake of inorganic carbon and nitrate by marine plankton and the Redfield ratio. Global Biogeochemical Cycles 8(1), 81–84.

Bates, N.R., Johnson, R.J., Michaels, A.F., Knap, A.H., 1996. Spatial variability of CO_2 species in the Sargasso Sea. Caribbean Journal of Science 32(3), 3030–304.

Bates, N.R., Michaels, A.F., Knap, A.H., 1996a. Alkalinity changes in the Sargasso Sea: geochemical evidence of calcification? Marine Chemistry 51, 347–358.

Bates, N.R., Michaels, A.F., Knap, A.H., 1996b. Seasonal and interannual variability of oceanic carbon dioxide species at the U.S. JGOFS Bermuda Atlantic Time-series Study (BATS) site. Deep-Sea Research II 43(2–3), 347–383.

Broecker, W.S., 1991. Keeping global change honest. Global Biogeochemical Cycles 5(3), 191–192.

Bronstein, I.N., Semendjajew, K.A., 1989. Taschenbuch der Mathematik, 24 ed. Verlag Harri Deutsch, Frankfurt/Main.

Carlson, C.A., Ducklow, H.W., Michaels, A.F., 1994. Annual flux of dissolved organic carbon from the euphotic zone in the northwestern Sargasso Sea. Nature 371, 405–408.

Carpenter, E., Price, C., 1977. Nitrogen fixation, distribution, and production of oscillatoria (trichodesmium) spp. in the western Sargasso and Caribbean Seas. Limnology and Oceanography 22, 60–72.

Carpenter, E.J., Scranton, M.I., Novelli, P.C., Michaels, A.F., 1987. Validity of N_2 fixation rate measurements in marine Oscillatoria (trichodesmium). Journal of Plankton Research 9(6), 1047–1056.

Craig, H., 1957. Isotopic standards for carbon and oxgyen and correction factors for mass-spectrometric analysis of carbon dioxide. Geochimica Cosmochimica Acta 12, 133–149.

Denman, K.L., Gargett, A., 1983. Time and space scales of vertical mixing and advection of phytoplankton in the upper ocean. Limnology and Oceanography 28(5), 801–815.

Siegel, D., Deuser, W., 1996. Trajectories of sinking particles in the Sargasso Sea: modelling of "statistical funnels" above deep-ocean sediment traps. Deep-Sea Research I 44(9–10), 1519–1541.

Dickson, A.G., 1990. Thermodynamics of the dissociation of boric acid in synthetic seawater from 273.15 to 318.15 K. Deep-Sea Research 37(5), 755–766.

Dickson, A.G., Millero, F.J., 1987. A comparison of the equilibrium constants for the dissociation of carbonic acid in seawater media. Deep-Sea Research 34(10), 1733–1743.

Dickson, A.G., Riley, J.P., 1979. The estimation of acid dissociation constants in seawater media from potentiometric titrations with strong base, II. The dissociation of phosphoric acid. Marine Chemistry 7, 101–109.

Dillon, T.M., Caldwell, D.R., 1980. The Batchelor spectrum and dissipation in the upper ocean. Journal of Geophysical Research 85(C4), 1910–1916.

Doney, S.C., 1996. A synoptic atmosphere surface forcing data set and physical upper ocean model for the U.S. JGOFS Bermuda Atlantic Time-Series Study site. Journal of Geophysical Research 101(C10), 25 615–25 634.

Doney, S.C., Glover, D.M., Najjar, R.G., 1996. A new coupled, one-dimensional biological–physical model for the upper ocean: applications to the JGOFS Bermuda Atlantic Time-series Study (BATS) site. Deep-Sea Research II 43(2–3), 591–624.

Druffel, E.R.M., Williams, P., Bauer, J.E., Ertel, J.R., 1992. Cycling of dissolved and particulate organic matter in the open ocean. Journal of Geophysical Research 97(C10), 15639–15659.

Duce, R., 1986. The impact of atmospheric nitrogen, phosphorus and iron species on marine biological productivity. In: Buat-Ménard. (Ed.), The role of Air–sea Exchange in Geochemical Cycling. Reidel, D., Hingham, MA, pp. 497–529.

Fasham, M.J.R., Ducklow, H.W., McKelvie, S.M., 1990. A nitrogen-based model of plankton dynamics in the oceanic mixed layer. Journal of Marine Research 48, 591–639.

Fink, R., 1996. Zur Kohlenstoffchemie des Ozeans und zur Modellierung des natürlichen Kohlenstoffkreislaufes. PhD thesis, Phys. Inst., Univ. of Bern, Bern, Switzerland.

Follows, M.J., 1996. Regional tracer and carbon cycle models. In: Ormerod, B. (Ed.), Ocean Storage of Carbon Dioxide. IEA Greenhouse Gas R&D Programme, Cheltenham, UK, pp. 53–70.

Follows, M.J., Williams, R.G., Marshall, J.G., 1996. The solubility pump of carbon in the subtropical gyre of the North Atlantic. Journal of Marine Research 54, 605–630.

Gregg, M.C., 1987. Diapycnal mixing in the thermocline: a review. Journal of Geophysical Research 92(C5), 5249–5286.

Gruber, N., 1997. Aspects of the marine carbon and nitrogen cycles and their perturbation by mankind: combining observations and models. PhD thesis, Phys. Inst., Univ. Bern, Bern, Switzerland.

Gruber, N., Keeling, C.D., 1998. Seasonal carbon cycling in the Sargasso Sea near Bermuda. Scripps Institution of Oceanography, Bulletin, 30, in press.

Gruber, N., Sarmiento, J.L., 1997. Global patterns of marine nitrogen fixation and denitrification. Global Biogeochemical Cycles 11(2), 235–266.

Heimann, M., Keeling, C.D., Tucker, C.J., 1989. A three dimensional model of atmospheric CO_2 transport based on observed winds: 3. Seasonal cycle and synoptic time scale variations. In: Peterson, D.H. (Ed.), Aspects of Climate Variability in the Pacific and the Western Americas, Geophysical Monograph Series 55, pp. 277–303. AGU, Washington, DC.

Hurtt, G.C., Armstrong, R.A., 1996. A simple ocean mixed layer ecosystem model calibrated with BATS data. Deep-Sea Research II 43(2–3), 653–683.

Isemer, H., Hasse, L., 1985. The Bunker Climate Atlas of the North Atlantic Ocean, Springer, Berlin.

Jenkins, W.J., Goldman, J.C., 1985. Seasonal oxygen cycling and primary production in the Sargasso Sea. Journal of Marine Research 43, 465–491.

Karl, D.M., Letelier, R., Hebel, D.V., Bird, D.F., Winn, C.D., 1992. Trichodesmium blooms and new production in the North Pacific gyre. In: Carpenter, E.J. (Ed.), Marine Pelagic Cyanobacteria: Trichodesmium and other Diazotrophs. Kluwer Academic Publishers, Dordrecht, pp. 219–237.

Keeling, C.D., 1993. NATO lecture 2: Surface ocean CO_2, In: Heimann, M. (Ed.), The Global Carbon Cycle. Springer, New York, pp. 413–430.

Keeling, C.D., Bacastow, R.B., Carter, A.F., Piper, S.C., Whorf, T.P., Heimann, M., Mook, W.G., Roeloffzen, H., 1989. A three dimensional model of atmospheric CO_2 transport based on observed winds: 1. Analysis of observational data. In: Peterson, D.H. (Ed.), Aspects of Climate Variability in the Pacific and the Western Americas, Geophysical Monograph Series 55. AGU, Washington, DC, 165–237.

Knap, A.H., Michaels, A.F., Dow, R.L., Johnson, R.J., Gundersen, K., Sorensen, J.C., Close, A.R., Hammer, M., Knauer, G.A., Lohrenz, S.E., Asper, V.A., Tuell, M., Ducklow, H., Quinby, H., Brewer, P., Bidigare, R., 1992. Data report for BATS 13–BATS 24, October 1989–September 1990. Bermuda Bio. Sta. Res., Inc., U.S. Joint Global Ocean Flux Study, Technical Report BATS data report B-2. U.S. JGOFS Planning Office, Woods Hole, MA.

Knap, A.H., Michaels, A.F., Dow, R.H., Johnson, R.J., Gundersen, K., Sorensen, J.C., Close, A.R., Howse, F., Hammer, M., Bates, N., Lohrenz, G.A.K.S.E., Asper, V.A., Tuell, M., Ducklow, H., Quinby, H., 1993. Data report for BATS 25–BATS 36, October 1990–September 1991. Bermuda Bio. Sta. Res., Inc., U.S. Joint Global Ocean Flux Study, Technical Report BATS data report B-3. U.S. JGOFS Planning Office, Woods Hole, MA.

Knap, A.H., Michaels, A.F., Dow, R.L., Johnson, R.J., Gundersen, K., Sorensen, J.C., Close, A.R., Howse, F., Bates, N., Best, M., Hammer, M., Doyle, A., 1994. Data report for BATS 37–BATS 48, October 1991–September 1992. Bermuda Bio. Sta. Res., Inc., U.S. Joint Global Ocean Flux Study, Techical Report BATS data report B-4. U.S. JGOFS Planning Office, Woods Hole, MA.

Large, W.G., McWilliams, J.C., Niiler, P.P., 1986. Upper ocean thermal response to strong autumnal forcing of the Northeast Pacific. Journal of Physical Oceanography 16, 1524–1550.

Laws, E.A., 1991. Photosynthetic quotients, new production and net community production in the open ocean. Deep-Sea Research 38(1), 143–167.

Ledwell, J.R., Watson, A.J., Law, C.S., 1993. Evidence for slow mixing across the pycnocline from an open-ocean tracer-release experiment. Nature 364, 701–703.

Levitus, S., 1982. Climatological atlas of the world ocean. Geophysical Fluid Dynamics Laboratory, NOAA Professional Paper, 13, Princeton, NJ.

Liss, P.S., Merlivat, L., 1986. Air–sea exchange rates: introduction and synthesis. In: Buat-Ménard, P. (Ed.), The Role of Air–Sea Exchange in Geochemical Cycling, Reidel, D., Hingham, MA, 113–127.

Lohrenz, S.E., Knauer, G.A., Asper, V.L., Tuel, M., Michaels, A.F., Knap, A.H., 1992. Seasonal variability in primary production and particle flux in the northwestern Sargasso Sea: U.S. JGOFS Bermuda Atlantic Time-series Study. Deep-Sea Research 39(7/8), 1373–1391.

Lueker, T.J., Keeling, C.D., Guenther, P.R., Mook, W.G., Wahlen, M., 1997. A twelve year record of inorganic carbon variations in surface ocean water near bermuda. Global Biogeochemical Cycles, submitted.

Lynch-Stieglitz, J., Stocker, T.F., Broecker, W.S., Fairbanks, R.G., 1995. The influence of air-sea exchange on the isotopic composition of oceanic carbon: observations and modeling. Global Biogeochemical Cycles 9(4), 653–665.

Maier-Reimer, E., Hasselmann, K., 1987. Transport and storage of CO_2 in the ocean – an inorganic ocean-circulation carbon cycle model. Climate Dynamics 2, 63–90.

Maier-Reimer, E., Mikolajewicz, U., Winguth, A., 1996. Future ocean uptake of CO_2: interaction between ocean circulation and biology. Climate Dynamics 12, 711–721.

Manabe, S., Stouffer, R.J., 1993. Century-scale effects of increased atmospheric CO_2 on the ocean-atmosphere system. Nature 364, 215–218.

Marchal, O., 1996. Cycle saisonnier du CO_2 dans la zone euphotique marine – une étude dans la mer des Sargasses. PhD thesis, Université Paris 6, Paris.

Marchal, O., Monfray, P., Bates, N.R., 1996. Spring–summer imbalance of dissolved inorganic carbon in the mixed layer of the northwestern Sargasso Sea. Tellus Ser. B. 48, 115–134.

Martin, J.H., Knauer, G.A., Karl, D.M., Broenkow, W.W., 1987. Vertex: carbon cycling in the northeast Pacific. Deep-Sea Research 34(2), 267–285.

Matear, R.J., 1995. Parameter optimization and analysis of ecosystem models using simulated annealing: a case study at station P. Journal of Marine Research 53, 571–607.

McAllister, C.D., Parsons, T.R., Stephens, K., Strickland, J.D.H., 1961. Measurements of primary production in coastal sea water using a large-volume plastic sphere. Limnology and Oceanography 6, 237–258.

McCarthy, J., Carpenter, E., 1983. Nitrogen cycling in near-surface waters of the open ocean. In: Carpenter, E., Capone, D. (Eds.), Nitrogen in the Marine Environment, Academic Press, San Diego, CA, 487–512.

Menzel, D.W., Ryther, J.H., 1961. The annual cycle of primary production in the Sargasso Sea off Bermuda. Deep-Sea Research 6, 351–367.

Menzel, D.W., Ryther, J.H., 1961. Annual variations in primary production of the Sargasso Sea off Bermuda. Deep-Sea Research 7, 282–288.

Michaels, A.F., Bates, N.R., Buesseler, K.O., Carlson, C.A., Knap, A.H., 1994. Carbon-cycle imbalances in the Sargasso Sea. Nature 372, 537–540.

Michaels, A.F., Knap, A.H., 1996. Overview of the U.S. JGOFS Bermuda Atlantic Time-series Study and the Hydrostation S program. Deep-Sea Research II 43(2–3), 157–198.

Michaels, A.F., Knap, A.H., Dow, R.L., Gundersen, K., Johnson, R.J., Sorensen, J., Close, A., Knauer, G.A., Lohrenz, S.E., Asper, V.A., Tuel, M., Bidigare, R., 1994b. Seasonal patterns of ocean biogeochemistry at the U.S. JGOFS Bermuda Atlantic Time-series Study site. Deep-Sea Research II 41(7), 1013–1038.

Michaels, A.F., Olson, D., Sarmiento, J.L., Ammerman, A., Fanning, K., Jahnke, R., Knap, A.H., Lipschultz, R., Prospero, J., 1996. Inputs, losses and transformations of nitrogen and phosphorus in the pelagic North Atlantic Ocean. Biogeochemistry 35, 181–226.

Michaels, A.F., Siegel, D.A., Johnson, R.J., Knap, A.H., Galloway, J.N., 1993. Episodic input of atmospheric nitrogen to the Sargasso Sea: contributions to new production and phytoplankton blooms. Global Biogeochemical Cycles 7(2), 339–351.

Millero, F.J., 1995. Thermodynamics of the carbon dioxide system in the oceans. Geochimica Cosmochimica Acta 59(4), 661–677.

Millero, F.J., Byrne, R.H., Wanninkhof, R., Feely, R., Clayton, T., Murphy, P., Lamb, M.F., 1993. The internal consistency of CO_2 measurements in the equatorial Pacific. Marine Chemistry 44, 269–280.

Mook, W.G., Bommerson, J.C., Staverman, W.H., 1974. Carbon isotope fractionation between dissolved bicarbonate and gaseous carbon dioxide. Earth and Planetary Science Letters 22, 169–176.

Mook, W.G., Grootes, P.M., 1973. The measuring procedure and corrections for the high-precision mass-spectrometric analysis of isotopic abundance ratios, especially referring to carbon, oxygen and nitrogen. International Journal of Mass Spectrometry Physics 12, 273–298.

Musgrave, D.L., Chou, J., Jenkins, W.J., 1988. Application of a model of upper-ocean physics for studying seasonal cycles of oxygen. Journal of Geophysical Research 93(C12), 15 679–15 700.

Olbers, D., Wenzel, M., Willebrand, J., 1985. The inference of North Atlantic circulation patterns from climatological hydrographic data. Reviews of Geophysics 23, 313–356.

Oudot, C., 1989. O_2 and CO_2 balances approach for estimating biological production in the mixed layer of the tropical Atlantic Ocean (Guinea Dome area). Journal of Marine Research 47, 385–409.

Owens, N.J.P., Galloway, J.N., Duce, R.A., 1992. Episodic atmospheric nitrogen deposition to oligotrophic oceans. Nature 357, 397–399.

Platt, T., Harrison, W.G., 1985. Biogenic fluxes of carbon and oxygen in the ocean. Nature 318, 55–58.

Platt, T., Harrison, W.G., Lewis, M.R., Li, W.K.W., Sathyendranath, S., Smith, R.E., Vezina, A.F., 1989. Biological production of the oceans: the case for a consensus. Marine Ecology Progress Series 52, 77–88.

Press, W., Teukolsky, S., Vetterling, W., Flannery, B., 1992. Numerical Recipes, 2nd ed. Cambridge University Press, Cambridge.

Rau, G.H., Takahashi, T., Marais, D.J.D., 1989. Latitudinal variations in plankton $\delta^{13}C$: implications for CO_2 and productivity in past oceans. Nature 341, 516–518.

Redfield, A.C., Ketchum, B.H., Richards, F.A., 1963. The influence of organisms on the composition of sea-water. In: Hill, M.N. (Ed.), The Sea, vol. 2, Wiley-Interscience, New York, 26–77.

Rubinstein, R.Y., 1981. Simulation and the Monte Carlo method. Wiley, New York.

Sambrotto, R.N., Savidge, G., Robinson, C., Boyd, P., Takahashi, T., Karl, D.M., Langdon, C., Chipman, D., Marra, J., Codispoti, L., 1993. Elevated consumption of carbon relative to nitrogen in the surface ocean. Nature 363, 248–250.

Sarmiento, J.L., 1991. Oceanic uptake of anthropogenic CO_2: the major uncertainties. Global Biogeochemical Cycles 5(4), 309–313.

Sarmiento, J.L., LeQuéré, C., 1996. Oceanic carbon dioxide uptake in a model of century-scale global warming. Science 274, 1346–1350.

Sarmiento, J.L., Murnane, R., LeQuéré, C., 1995. Air–sea CO_2 transfer and the carbon budget of the North Atlantic. Philosophical Transactions of the Royal Society of London B, 348, 211–219.

Sarmiento, J.L., Orr, J.C., Siegenthaler, U., 1992. A perturbation simulation of CO_2 uptake in an ocean general circulation model. Journal of Geophysical Research 97(C3), 3621–3645.

SCOR, 1987. The joint global ocean flux study: background, goals, organization, and next steps. Report of the International Scientific Planning and Coordination Meeting for Global Ocean Flux Studies. Dalhousie Univ., Technical Report, Halifax, Nova Scotia, Canada.

Siegel, D.A., Iturriaga, R., Bidigare, R.R., Smith, R.C., Pak, H., Dickey, T.D., Marra, J., Baker, K.S., 1990. Meridional variations of the springtime phytoplankton community in the Sargasso Sea. Journal of Marine Research 48, 379–412.

Siegel, D.A., Michaels, A.F., Sorensen, J.C., O'Brien, M.C., Hammer, M.A., 1995. Seasonal variability of light availability and utilization in the Sargasso Sea. Journal of Geophysical Research 100(C5), 8695–8713.

Siegenthaler, U., Joos, F., 1992. Use of a simple model for studying oceanic tracer distributions and the global carbon cycle. Tellus Series B 44, 186–207.

Siegenthaler, U., Sarmiento, J.L., 1993. Atmospheric carbon dioxide and the ocean. Nature 365, 119–125.

Spitzer, W.S., Jenkins, W.J., 1989. Rates of vertical mixing, gas exchange and new production: Estimates from seasonal gas cycles in the upper ocean near Bermuda. Journal of Marine Research 47, 169–196.

Sprintall, J., Tomczak, M., 1992. Evidence of barrier layer in the surface layer of the tropics. Journal of Geophysical Research 97(C5), 7305–7316.

Stocker, T.F., Broecker, W.S., Wright, D.G., 1994. Carbon uptake experiments with a zonally averaged global ocean circulation model. Tellus Series B 46, 103–122.

Stocker, T.F., Schmittner, A., 1997. Influence of CO_2 emission rates on the stability of the thermohaline circulation. Nature 388, 862–865.

Takahashi, T., Olafsson, J., Goddard, J.G., Chipman, D.W., Sutherland, S.C., 1993. Seasonal variation of CO_2 and nutrients in the high-latitude surface oceans: a comparative study. Global Biogeochemical Cycles 7(4), 843–878.

Talley, L.D., Raymer, M.E., 1982. Eighteen degree water variability. Journal of Marine Research 40 (Suppl), 757–775.

Tans, P.P., Fung, I.Y., Takahashi, T., 1990. Observational constraints on the global atmospheric CO_2 budget. Science 247, 1431–1438.

Toggweiler, J.R., 1993. Carbon overconsumption Nature 363, 210–211.

Toggweiler, J.R., 1994a. Anthropogenic CO_2: the natural carbon cycle reclaims center stage. Reviews in Geophysics (Suppl.), 1249–1252.

Toggweiler, J.R., 1994b. Vanishing in Bermuda. Nature 372, 505–506.

UNESCO, 1981. Background papers and supporting data on the practical salinity scale. UNESCO, UNESCO Technical Papers in Marine Science 37, Paris.

Uppström, L., 1974. The boron/chlorinity ratio of deep-sea water from the Pacific Ocean. Deep-Sea Research 21, 161–162.

Wanninkhof, R., 1992. Relationship between wind speed and gas exchange over the ocean. Journal of Geophysical Research 97(C5), 7373–7382.

Weiss, R., 1974. Carbon dioxide in water and seawater: the solubility of non-ideal gas. Marine Chemistry 2, 203–215.

Weiss, R.F., 1981. Determinations of carbon dioxide and methane by dual catalyst flame ionization chromatography and nitrous oxide by electron capture chromatography. Journal of Chromatographic Science 19, 611–616.

Williams, P.J.l., 1993. On the definition of plankton production terms. ICES Marine Science Symposium 197, 9–19.

Winn, C.D., Mackenzie, F.T., Carrillo, C.J., Sabine, C.L., Karl, D.M., 1994. Air–sea exchange in the North Pacific subtropical gyre: Implications for the global carbon budget. Global Biogeochemical Cycles 8(2), 157–163.

WMO/WDCGG, 1995. World Meteorological Organisation Global Atmosphere Watch World Data Centre for Greenhouses Data Report. Part A (Carbon Dioxide), GAW data, World Meteorological Organization, Global Atmosphere Watch, World Data Centre for Greenhouse Gases, Data report, 7, Tokyo.

Worthington, L.V., 1959. The 18° water in the Sargasso Sea. Deep–Sea Research 5, 297–305.